

## THESIS

# VOLATILITY AND OXIDATIVE REACTIVITY PROPERTIES OF DIESEL EXHAUST PARTICLES: ROLE OF FUEL, ENGINE LOAD, AND EMISSIONS CONTROL

Submitted by

Naman Sharma

Department of Mechanical Engineering

In partial fulfillment of the requirements

For the Degree of Master of Science

Colorado State University

Fort Collins, Colorado

Fall 2018

Master's Committee:

Advisor: Shantanu H. Jathar

John Volckens

Charles S. Henry

Copyright by Naman Sharma 2018

All Rights Reserved

## ABSTRACT

### VOLATILITY AND OXIDATIVE REACTIVITY PROPERTIES OF DIESEL EXHAUST PARTICLES: ROLE OF FUEL, ENGINE LOAD, AND EMISSIONS CONTROL

Diesel exhaust particles (DEP) are air pollutants that adversely affect air quality and human health. DEPs have been shown to be semi-volatile and hence they partition between the gas and particle phase. DEPs additionally are also very reactive and can directly or indirectly lead to the formation of reactive oxygen species inside the human body. The volatility and oxidative reactivity of DEP are not well understood and particularly uncertain when it comes to alternative fuels, engine load and modern emissions control devices.

In this study, we measured DEPs from a modern-day non-road diesel engine for two different fuels (conventional diesel and soy-based biodiesel), two different engine loads (idle and 50% load), and with and without emissions control devices. The DEPs were collected on a combination of bare quartz (BQ), Teflon<sup>®</sup> and quartz behind Teflon<sup>®</sup> (QBT) filters for approximately 8 different dilution ratios. We also measure gaseous pollutants like CO, CO<sub>2</sub>, NO<sub>x</sub>, O<sub>2</sub> and THC from diesel engine over the fuel-load-emissions control combinations. These collected filters were later used offline to determine volatility, composition and oxidative reactivity of DEPs.

The Teflon<sup>®</sup> filters were used to determine gravimetric mass, inorganic ions, water soluble organic carbon, black carbon and oxidative reactivity. The quartz filters were used to determine trace metals, organic carbon, elemental carbon, volatility and oxidative reactivity. Differences

between the bare quartz and quartz behind Teflon<sup>®</sup> filter were used to infer the volatility. A dithiothreitol chemical assay was used to measure the oxidative reactivity of DEP's. This study is an effort to determine the link between PM composition, volatility and oxidative reactivity for two different fuel combination, two different engine load and influence on emission control systems.

The use of biodiesel fuel tends to decrease NO<sub>x</sub>, THC and CO<sub>2</sub> emissions factors when compared against diesel fuel. However, we see an increase in CO emissions factor for biodiesel fuel. The NO<sub>x</sub> and CO emission factor increased as we go from idle to 50% load conditions but remain almost same for CO<sub>2</sub> and decreases significantly for THC. The emissions control system decreases THC and NO<sub>x</sub> emissions for both ideal and load conditions. The estimated volatility distribution did not change with fuel, engine load, or emissions control system and only one distribution could be used in atmospheric models. In contrast, the oxidative reactivity of DEPs from the use of biodiesel fuel seemed to be lower (~83 and 97%) than that for diesel fuel on an emission factor basis. The oxidative reactivity for different engine loads does not seem to show any trend on a per PM basis unlike some other previous studies. However, the oxidative reactivity was lower for 50% load condition (~67%) as compared to idle conditions on an emissions factor basis. The use of a diesel particulate filter (DPF), which is an emissions control device, significantly reduced (~93% ) the oxidative reactivity of DEPs. This study also observed the influence of semi-volatile vapors (QBT), which contributed nearly 25% of the oxidative reactivity of particles and vapors (BQ). Finally, the oxidative reactivity of DEPs was compared for filter and solvent membrane effects. The oxidative reactivity of DEPs extracted from Teflon<sup>®</sup> was found out to be higher by a factor of ~2 when compared with the reactivity associated with

quartz membrane filter. The oxidative reactivity for organic solvent is higher and show very strong response than water-based solvent especially for biodiesel exhaust particles.

## ACKNOWLEDGMENTS

I would like to thank my advisor Dr. Shantanu Jathar for being a fantastic instructor, teaching assistantship supervisor, and thesis advisor. I believe his valuable inputs allowed me to excel through my time under his instruction. I really feel blessed to have had him as a mentor during my master's program.

I would also like to thank Dr. Charles Henry for allowing me to use his laboratory that helped me in the completion of this thesis. I would also like to thank Dr. Christian L'Orange, Dr. Kevin Klunder, and Dr. Amy Sullivan for helping me with different trainings that again helped me to complete this thesis. The LAQR (Laboratory of Air Quality Research) group support especially Ali, Shiva, Cody and Liam for helping me with technical and non-technical support during my research.

Lastly, I would like to thank my parents and friends for their support and confidence in me to achieve higher goals in life.

## TABLE OF CONTENTS

ABSTRACT.....	ii
NOMENCLATURE .....	viii
LIST OF FIGURES .....	ix
LIST OF TABLES .....	xii
1 Introduction.....	1
2 Methods.....	8
2.1 Engine Experiments .....	8
2.1.1 Engine Details.....	8
2.1.2 Experimental Setup.....	9
2.1.3 Gas-Phase Measurements .....	11
2.1.4 Particle Collection and Measurements .....	12
2.2 Laboratory Measurements and Primary Analysis .....	15
2.2.1 PM <sub>2.5</sub> Gravimetric Mass .....	16
2.2.2 Organic and Elemental Carbon.....	17
2.2.3 Inorganic and Water-Soluble OC .....	18
2.2.4 Trace Metals .....	19
2.2.5 Dithiothreitol Assay.....	20
2.2.6 SootScan Black Carbon .....	24
2.3 Secondary Analysis .....	25
3 Results.....	28
3.1 Emission Factors for Gaseous Pollutants .....	28
3.2 Emission Factors for Particle Pollutants .....	30
3.3 PM <sub>2.5</sub> Composition and Closure .....	31
3.4 POA Volatility.....	37
3.5 Oxidative Reactivity.....	40

3.5.1 Fuel and Engine Load Effects .....	40
3.5.2 Emissions Control Effects .....	44
3.5.3 Understanding Links to PM <sub>2.5</sub> Composition.....	45
4 Discussion and future work .....	53
References.....	56
Appendix.....	70



## NOMENCLATURE

POA- Primary organic aerosol

OC- Organic carbon

EC- Elemental carbon

BC- Black carbon

EF- Emissions factor

Xp- Fractions of organic carbon in particle phase

DEP- Diesel exhaust particle

DPF- Diesel particulate filter

DOC- Diesel oxidation catalyst

BQ- Bare quartz

QBT- Quartz behind Teflon®

QBQ- Quartz behind quartz

HB- Handling blank

DB- Dynamic blank

DTT- Dithiothreitol

## LIST OF FIGURES

Figure 1: Schematic visualizing the experimental setup and particle collection. MFC = mass flow controller, TC = thermocouple, PP = pressure probe, TP = temperature probe, C2.5 = PM2.5 cyclone .....	15
Figure 2: Emission factors for (a) CO <sub>2</sub> , (b) CO, (c) NO <sub>X</sub> and (d) THC for the various fuel-engine load-emissions control combinations in units of g kg-fuel-1.....	28
Figure 3: Emission factors for (a) PM <sub>2.5</sub> , (b) POA, and (c) EC in units of g kg-fuel-1 and the (d) EC:POA ratio for the various fuel-engine load-emissions control combinations. Panels include both the box plot and the individual data used to create the box plot. The box presents the 25th, 50th, and 75th percentile of the data and the whiskers present the lowest and highest values that are not outliers. Outliers are defined as points that lie three times beyond the interquartile range. Outliers in the DPF+DOC data are circled in magenta. Values smaller than zero are not shown. ....	33
Figure 4: Scatter plot comparing the measured mass concentrations of POA+EC against mass concentrations of PM <sub>2.5</sub> for all experiments performed in this work. The POA data have been artifact corrected. ....	35
Figure 5: (a) Scatter plot comparing mass concentrations of BC measured by the SootScan (SS) and PAX against mass concentrations of EC measured by the Sunset OC/EC analyzer for all experiments performed in this work. (b) Scatter plot comparing mass concentrations of BC measured by the SootScan (SS) against those measured by the PAX for all experiments performed in this work.....	37

Figure 6: Fraction of POA mass in the particle phase ( $X_p$ ) plotted against the POA mass concentrations for all experiments performed in this work. .... 38

Figure 7: Fraction of POA mass in the particle phase ( $X_p$ ) plotted against the POA mass concentrations for all experiments performed in this work. Panel (a) compares raw measurements against estimates based on the volatility distribution fits. Panel (b) compares estimates of  $X_p$  based on the volatility distribution fits against measurements using a scatter plot. Panel (c) compares predictions of  $X_p$  against those estimated by earlier work. .... 39

Figure 8: Measured oxidative reactivity of DEPs in two different units (a,c)  $\text{nmoles min}^{-1} \mu\text{g PM-1}$  and (b,d)  $\text{nmoles min}^{-1} \text{kg-fuel}^{-1}$ . The presented data are resolved by fuel (diesel=orange, biodiesel=blue) and engine load (idle=circle, load=triangle). Panels (a) and (b) capture fuel effects while panels (c) and (d) capture load effects. The black solid line connects the medians of the distributions that are compared and p-values are shown in italic with significant p-values underlined. .... 42

Figure 9: Measured oxidative reactivity of DEPs comparing experiments with and without the emissions control in two different units (a)  $\text{nmoles min}^{-1} \mu\text{g PM-1}$  and (b)  $\text{nmoles min}^{-1} \text{kg-fuel}^{-1}$ . The black solid line connects the medians of the distributions that are compared and p-values are shown in italic with significant p-values underlined. .... 44

Figure 10: Measured oxidative reactivity of DEPs in  $\text{nmoles min}^{-1} \text{kg-fuel}^{-1}$  regressed against emission factors for (a)  $\text{PM}_{2.5}$ , (b) EC, (c) particle+vapor OC, (d) particle OC, and (e) vapor OC. The dashed lines are linear fits to the data. .... 46

Figure 11: Scatter plot of the raw oxidative reactivity measurements in  $\mu\text{M min}^{-1}$  performed on unfiltered and filtered extracts prepared from all BQ filters. .... 48

Figure 12: Measured oxidative reactivity of DEPs resolved by phase of the material (particles+vapors and vapors) in two different units (a) nmoles min<sup>-1</sup> μg PM-1 and (b) nmoles min<sup>-1</sup> kg-fuel-1. The presented data are resolved by fuel (diesel=orange, biodiesel=blue) and engine load (idle=circle, load=triangle). The black solid line connects the medians of the distributions that are compared and p-values are shown in italic with significant p-values underlined. ....49

Figure 13: Scatter plot of the raw oxidative reactivity measurements in μM min<sup>-1</sup> performed on all paired BQ and QBT filters..... 50

Figure 14: Measured oxidative reactivity of DEPs in nmoles min<sup>-1</sup>μg PM-1 for select samples examining the influence of the (a) filter type (Teflon versus quartz) and (b) solvent (organic versus water). ....52

Figure 15:Compares DTT-oxidative reactivity for combustion sources and ambient measurement against our oxidative reactivity data in nmoles min<sup>-1</sup>μg PM-1. The color represents different fuel types and emissions control conditions and different markers are used for to represent different source studies. The ambient DTT data shown here is compiled into a box plot from table 5. (For references link to table 5.)..... 55

Figure 16:compares histogram plot for all sample and laboratory measurements in units of μM of DTT consumed min<sup>-1</sup>. ....73

## LIST OF TABLES

Table 1: List of the fuel-engine load-emissions control experiments performed in this work and their dilution ratio details. ....	10
Table 2: Description and details of the laboratory measurements performed for the various filters collected during the study. ....	15
Table 3: Details of the DTT assay performed in this work resolved by experiment type (fuel-engine load-emissions control combination), filter media, solvent used for extraction, and treatment of the extract (filtered versus unfiltered). ....	21
Table 4: Emission factors for CO, THC, NO <sub>x</sub> , PM <sub>2.5</sub> , POA, and EC compared against the 25 <sup>th</sup> -75 <sup>th</sup> percentile data compiled in May et al. <sup>70</sup> from a range of dynamometer <sup>71-74</sup> , on-road <sup>75,76</sup> , and tunnel studies <sup>77-79</sup> . ....	31
Table 5: Emission factors for POA, EC, inorganic compounds, and trace metals for all fuel-engine load combinations without emissions control. The inorganic ions and metals were not measured for the experiments with emissions control. ....	34
Table 6: Compilation of DTT-based oxidative reactivity measurements from engine and vehicle tests and ambient sampling. ....	70

## 1 Introduction

Combustion sources such as motor vehicles, electricity generating units, cookstoves, and wildfires emit fine particles or particulate matter smaller than 2.5 microns ( $PM_{2.5}$ ) as a result of incomplete combustion.  $PM_{2.5}$  is an important atmospheric pollutant that has large impacts on climate,<sup>1</sup> air quality,<sup>2</sup> and human health.<sup>3</sup> For instance,  $PM_{2.5}$  absorbs and scatters incoming solar radiation<sup>4</sup> and influences cloud lifetime and properties<sup>5,6</sup> to perturb the energy budget of the earth. Exposure to indoor and outdoor  $PM_{2.5}$  has been linked to seven million premature respiratory and cardiovascular deaths annually across the globe.<sup>7</sup> Yet, there are large uncertainties in quantifying the precise impact of  $PM_{2.5}$  on current and future climate and the mechanisms by which  $PM_{2.5}$  exposure results in adverse health outcomes. There is a need to better understand the atmospheric- and health-relevant properties of  $PM_{2.5}$  if we are to quantify and mitigate the environmental damages stemming from it.

Direct emissions of combustion-related  $PM_{2.5}$  are primarily composed of black/elemental carbon (BC/EC) and primary organic aerosol (POA), with minor contributions from inorganic compounds such as sulfate, nitrate, and ammonium and metals such as iron, zinc, and aluminium.<sup>8-3</sup> While BC/EC is widely believed to be non-volatile and reactive in the atmosphere, with a few exceptions, combustion-related POA is now understood to be semi-volatile, i.e., the organic compounds that constitute POA exist in an equilibrium between the gas and particle phases.<sup>9,10-12</sup> Combustion-related POA is likely to comprise of thousands of different organic compounds with very different physical and chemical properties. The distribution of POA in the gas and particle phases depends on the distribution of the vapor pressure of these organic compounds and, in theory, follows Raoult's law:  $P_i = x_i P_{L,0}^i$ , where  $P_i$  is the vapor pressure of

the organic compound above the particle surface,  $x_i$  is the mole fraction of the organic compound in the particle phase, and  $P_{L,0}^i$  is the pure saturation vapor pressure of the organic compound.<sup>13</sup> According to Raoult's law, dilution should reduce the partial pressure of the organic compounds in the gas phase and result in evaporation of the organic compounds in the particle phase to reestablish equilibrium. As the saturation vapor pressure varies with temperature based on the Clausius-Clapeyron equation, the partitioning of the organic compounds between the gas and particle phases will be perturbed with an increase in temperature leading to evaporation of particle mass and a decrease in temperature leading to condensation of gas-phase species into the particle phase. Dilution from atmospheric mixing and variations in ambient temperature are hence expected to alter the gas/particle partitioning of POA, which in turn controls the fate, lifetime, and impacts of POA in the atmosphere.

POA in diesel exhaust, similar to that from gasoline exhaust,<sup>10</sup> biomass burning,<sup>11</sup> and food cooking,<sup>14</sup> has been previously found to be semi-volatile.<sup>12</sup> Lipsky and Robinson<sup>15</sup> and Robinson et al.<sup>9</sup> used a small diesel generator and a isothermal dilution system to study the change in POA mass emissions with dilution that simulated atmospheric mixing. Both found that dilution to atmospherically-relevant concentrations ( $10 \mu\text{g m}^{-3}$ ) resulted in ~80% of the diesel POA to evaporate. Building on this initial work, the same diesel generator was used in two follow up studies. Grieshop et al.<sup>16</sup> used a thermodenuder in addition to a isothermal dilution system to constrain the gas/particle partitioning of diesel exhaust POA at even lower atmospheric concentrations of POA ( $<10 \mu\text{g m}^{-3}$ ) while Ranjan et al.<sup>17</sup> used an environmental chamber instead of a dilution system and validated observations from the earlier work. May et al.<sup>11</sup> investigated the gas/particle partitioning of POA emissions from two medium-duty trucks, three heavy-duty trucks, and one transportation refrigeration unit operated over a specific drive cycle

(e.g., transient, high speed, idle) using four independent but complementary methods: positive artifact on quartz filters, dilution between a constant volume sampler and an environmental chamber, thermal desorption / gas chromatography mass spectrometry, and thermal denuding. Results from the first three methods agreed with each other and suggested that at atmospherically-relevant concentrations of  $10 \mu\text{g m}^{-3}$  the POA mass emissions measured in the constant volume sampler would be reduced by one-half to two-thirds. The thermal denuding data suggested that about 20% of the POA mass measured in the constant volume sampler was possibly non-volatile. Li et al.<sup>18</sup> measured the gas/particle partitioning of POA emitted by a mixture of gasoline and diesel vehicles in a traffic tunnel in Pittsburgh, PA and observed that the partitioning of ambient POA was qualitatively similar to the partitioning observed with POA from source/laboratory testing of gasoline and diesel vehicles. This suggested that laboratory parameterizations could be used to model POA gas/particle partitioning directly in atmospheric models.<sup>10-12</sup> It is clear that diesel exhaust POA is semi-volatile but prior work has mostly focused on emissions from a small generator at a specified load and averaged emissions over a vehicle drive cycle. There are few data on diesel engine operation across engine loads. Further, with wider adoption of alternative fuels for diesel engines (e.g., biodiesel) and the requirement of emissions control systems to meet current emissions standards (e.g., Tier 2 for on-road, and Tier 4 for off-road), there is a need to investigate the semi-volatile behavior of POA with changes in fuel and addition of emissions control systems.

Exposure to diesel exhaust particles (DEPs) is known to have range of adverse health effects and has been extensively studied by toxicologists and epidemiologists alike. Toxicological studies using animal models suggest that DEPs have effects that range from obesity<sup>19</sup> to heart failure<sup>20</sup> while epidemiological studies have linked DEPs to diseases from lung cancer<sup>21</sup> to ischemia.<sup>22</sup>



Although human health effects from DEP exposure are widely reported, the mechanisms by which DEPs, and generally PM<sub>2.5</sub>, affect human health remain uncertain.<sup>4</sup> There is growing body of evidence that suggests that PM directly or indirectly through the production of reactive oxygen species (ROS; e.g., superoxide, hydroxyl radical, hydrogen peroxide) on the surface or within human cells, reduces the antioxidant loading in the human body.<sup>23</sup> The reduction of antioxidants can impose oxidative stress on human cells leading to inflammation and offers a mechanistic pathway that connects PM exposure to respiratory and cardiovascular diseases. The potential of PM to impose oxidative stress on human cells or the so-called oxidative reactivity of PM has been increasingly linked to poor health outcomes. Weichenthal and coworkers in a large study that included fifteen or more cities in the Ontario province in Canada found associations between the oxidative potential of PM and emergency room visits for respiratory illness<sup>24</sup> and myocardial infarction.<sup>25</sup> However, not all studies have found similar associations.<sup>26–28</sup>

The oxidative reactivity of PM has been measured using both acellular and cellular assays. Most acellular assays have been performed with dithiothreitol (DTT) since DTT is a thiol that resembles common antioxidants found in the human body and the assay is relatively easy to perform with basic analytical chemistry methods. Studies have also used ascorbic acid<sup>29</sup> and glutathione<sup>30</sup> as candidate molecules although these studies are less common compared to those performed with DTT. An acellular assay is typically performed by extracting the PM<sub>2.5</sub> collected on a filter with water or an organic solvent and reconstituting the PM<sub>2.5</sub> in a buffer solution at a pH (7.4) and temperature (37 °C) level representative of the human body. The PM<sub>2.5</sub> is then allowed to react with the candidate molecule and the decay of the molecule with time is recorded. The oxidative reactivity is quantified as the decay of the candidate molecule (e.g., DTT) with time (e.g., nmoles min<sup>-1</sup> or nmoles min<sup>-1</sup> μg PM<sup>-1</sup>) but the units have no physical

meaning in relation to human health effects and can only be interpreted in a relative sense. Cellular assays are typically harder to perform but offer a more health-relevant measurement compared to acellular assays. Regardless, the DTT-based oxidative reactivity measurement is emerging as an important metric to study the adverse effects of DEPs and PM<sub>2.5</sub> on human health.

Numerous studies over the past decade have focused on the measurement of the oxidative reactivity of DEPs and we highlight a few of those below. Geller et al.<sup>31</sup> in one of the first recorded studies, measured the oxidative reactivity of DEPs from a light-duty vehicle using a DTT assay and found that while the use of diesel particulate filter (DPF) they observe a decrease in PM emission by a factor of 25, the decrease in oxidative reactivity was only by a factor of 8, suggesting that many PM components were not efficiently removed by diesel particulate filter . Biswas et al.<sup>32</sup> measured the oxidative reactivity of DEPs from a suite of medium- and heavy-duty vehicles equipped with various emissions control technologies (e.g., diesel particulate filter, diesel oxidation catalyst, selective catalytic reduction units) using a DTT assay and found that the use of emissions control technology significantly (60-98%) reduced the oxidative reactivity of DEPs when expressed on a per mile basis. They also found that the oxidative reactivity of DEPs was reduced (50-100%) by thermally denuding the DEPs, implying that the oxidative reactivity was linked to the removal of semi-volatile organic compounds. Cheung and coworkers<sup>33</sup> undertook a study similar to Biswas et al.<sup>32</sup> but focused on the oxidative reactivity of PM<sub>2.5</sub> emitted by gasoline, diesel, and biodiesel light-duty vehicles and measured the oxidative reactivity via a DTT and a rat alveolar macrophage assay. They found that use of biodiesel fuel and emissions control devices reduced the oxidative reactivity of DEPs. They also found that the oxidative reactivity correlated strongly with organic compounds such as organic acids,

polycyclic aromatic hydrocarbons (PAHs), hopanes, and steranes constituting DEPs similar to Biswas et al.<sup>32</sup> Consistent with the three earlier studies, Kooter et al.<sup>34</sup> measured the oxidative reactivity of PM from a heavy duty truck engine and observed a 95% decrease in the oxidative reactivity with the use of biodiesel or a DPF that was linked to proportional decreases in EC and PAHs. McWhinney et al.<sup>35</sup> measured the oxidative reactivity of DEPs using the DTT assay and found that filtering the DEP-in-water extract resulted in a significant decrease in the oxidative reactivity, implying that the oxidative reactivity was attributable to the filterable components of PM that possibly include black carbon (BC). Finally, Stevanovic et al.<sup>36</sup> quantified the oxidative reactivity of DEPs by measuring ROS production, which was found to correlate with oxygenated organic compounds in DEPs. It appears that both organic compounds and elemental/black carbon play an important role in controlling the oxidative reactivity of DEPs but more detailed studies are needed to separate their relative contributions. Furthermore, most prior studies with DEPs have produced a normalized DTT oxidative reactivity (i.e., nmoles min<sup>-1</sup> μg PM<sup>-1</sup>) larger than that observed for typical ambient PM, placing emphasis on the study and mitigation of DEPs compared to particles from other sources.

A much wider body of literature has investigated the oxidative reactivity of combustion-related and ambient PM and attempted to link the oxidative reactivity measurement to the sources and composition of PM. Verma and coworkers measured the oxidative reactivity<sup>37</sup> and toxicity<sup>38</sup> of PM in the southeast US and found that both measures correlated with hydrophobic organic compounds in PM but showed weak or no association with metals. In Atlanta, GA, Verma et al.<sup>38</sup> found that secondary organic aerosol in the summer and biomass burning in the winter contributed to nearly half of the observed oxidative reactivity in ambient PM samples. In contrast to the findings of Verma and coworkers, Charrier and coworkers<sup>39,40</sup> have found that certain

transition metals such as copper and manganese and quinones such as phenanthrenequinone (PQN) can efficiently oxidize DTT and that their concentrations in ambient PM were sufficient to explain the entire observed oxidative reactivity of ambient PM. Saffari et al.<sup>41</sup> reviewed oxidative reactivity measurements made in six different cities across the globe and found that the oxidative reactivity correlated with smaller particle sizes, transition metals, water soluble organic carbon, and photochemical aging.

In this work, we studied the volatility and oxidative reactivity properties of diesel exhaust particles (DEPs) from a modern-day diesel engine under varying fuel, engine load, and emissions-control configurations. The volatility of primary organic aerosol was investigated using two independent techniques: positive artifacts on quartz filters and thermal desorption gas chromatography mass spectrometry. The oxidative reactivity of DEPs was investigated using the dithiothreitol assay. The dissemination of our work is organized in the subsequent chapters with the following structure. In Chapter 2, we discuss the experimental setup used to gather DEP filter samples from the tailpipe of a modern-day diesel engine and follow that with a description of the analytical methods used to determine the composition and oxidative reactivity of DEPs. In Chapter 3, we first present an overview of the gas- and particle-phase emissions and later present and discuss the volatility and oxidative reactivity measurements. In Chapter 4, we summarize the major findings, highlight uncertainties in current work, and offer recommendations for future work.

## 2 Methods

In this work, we studied the volatility and oxidative reactivity properties of diesel exhaust particles (DEPs) from a modern-day diesel engine under varying fuel, engine load, and emissions control configurations. The sampling study was performed as part of the Diesel Exhaust Fuel and Control (DEFCON) study conducted at Colorado State University between October 2015 and March 2016 and the laboratory measurements were performed between the May 2016 and December 2017. Below, we present details about the engine experiments and laboratory measurements and analysis.

### 2.1 Engine Experiments

#### 2.1.1 Engine Details

We used a 4-cylinder, turbocharged and intercooled, 4.5 L, 175 hp, John Deere 4045H PowerTech Plus engine, a generic engine commonly used in applications ranging from stationary power generation to agricultural and construction equipment. The engine was mounted on an engine dynamometer (Midwest Inductor Dynamometer 1014A) capable of applying a steady-state load on the engine. The stock engine met the Tier 3 emissions standards for off-road engines. An emissions control system consisting of a diesel oxidation catalyst (DOC) and a diesel particulate filter (DPF) were retrofitted on the exhaust system to meet off-road interim Tier 4 emissions standards but the engine was not recalibrated to optimize performance and emissions. This engine has been used in several studies in the past to: (i) understand the influence of alternative fuels on engine performance and tailpipe emissions<sup>42,43</sup> (ii) understand differences in the particle toxicity from diesel and biodiesel fuels,<sup>44</sup> (iii) study photochemical formation of secondary organic aerosol and organic acids in oxidation flow reactors<sup>45,46</sup> (iv)

quantify the emissions and formation of isocyanic acid in diesel exhaust<sup>47,48</sup> and (v) measure the ability of diesel exhaust particles to form ice nuclei.<sup>49</sup> In Figure 1 we draw a schematic to represent the engine used in this study and labels the key components that will be repeatedly mentioned in this thesis.

### **2.1.2 Experimental Setup**

Table 2 lists all the laboratory measurements done divided among two-channel Teflon<sup>®</sup>-quartz arrangement, used to sample the tailpipe emissions from the diesel engine. Emissions from the tailpipe were sampled through an isokinetic probe into a Hildemann-style dilution sampler<sup>50</sup> using activated charcoal- and HEPA-filtered clean air. The tailpipe emissions were drawn into the isokinetic probe and transferred to the dilution sampler using 15 feet of Silcosteel<sup>®</sup> tubing heated to 150 °C. The chemical passivation of the tube walls using SilcoNert<sup>®</sup> 1000 and heating of the tube outer surface were done to prevent loss of semi-volatile and intermediate volatility organic compounds to the tube walls. However, the use of SilcoNert<sup>®</sup> doesn't seem to do the trick. This gap in literature needs to be examined in future work.<sup>51</sup> The amount of clean air mixed with the exhaust (aka dilution air) was varied using a needle valve that throttled the suction on the pump used to run the dilution sampler. This method produced varying dilution ratios (ratio of clean air to exhaust), ranging from slightly under 4 to up to 400. For each experiment, that was some combination of fuel, engine load, and emissions control, the dilution ratio was varied between five to seven steps to produce different absolute concentrations of the pollutants and to assess the volatility of the organic fraction of the diesel exhaust particles (more details are provided in Section 2.3). The diluted exhaust was channeled into the top of a 300 L stainless steel residence tank, which was then used as a reservoir to sample the emissions using a host of instruments (details in the Section 2.2). The flow rates in the residence tank were such

that the diluted exhaust had a residence time of at least 4 mins, sufficient to achieve thermal (i.e., temperature) and thermodynamic (i.e., gas/particle partitioning) equilibrium.

The engine was operated in different fuel, engine load, and emissions control combinations. Two different fuels were used: (i) off-road, red dyed, diesel sourced from Team Petroleum (Fort Collins, CO) and (ii) soy-based biodiesel sourced from Emergent Green Energy (Minneola, KS). The engine was run at two different loads: (i) idle conditions that corresponded to a 0% load - 0 kW at 900 rpm and (ii) load conditions that corresponded to 50% load - 60 kW at 2200 rpm. The stock engine had an exhaust gas recirculation system to reduce NO<sub>x</sub> emissions, which was not altered during this study. The engine was operated with and without the emissions control system that consisted of the DOC (that oxidized unburned hydrocarbons and CO) and DPF (that filtered fine particles). Each combination of fuel, engine load, and emissions control was run, with repeats performed for many, if not all, of the combinations. For each fuel-engine load-emissions control combination, we performed measurements at multiple dilution ratios. The experimental matrix is tabulated in Table 1.

Table 1: List of the fuel-engine load-emissions control experiments performed in this work and their dilution ratio details.

<i>Fuel-Load-Emissions Control</i>	<i># of Experiment Days</i>	<i>Dilution Ratio Range</i>	<i>Number of Unique Dilution Ratio Experiments</i>
Diesel-Idle-None (Tier 3)	3	3-468	19
Diesel-Load-None (Tier 3)	3	4-222	11
Biodiesel-Idle-None (Tier 3)	3	3-200	16
Biodiesel-Load-None (Tier 3)	3	3-127	10
Diesel-Idle-DPF+DOC (Tier 3)	1	3-107	4
Diesel-Load-DPF+DOC (Tier 4)	2	2-8	5

Operationally, existing fuel in the fuel tank was siphoned and replaced with the test fuel, unless the existing fuel and test fuel were identical. The engine was started and warmed for at least 15 minutes before setting the desired engine load condition to ensure the fuel from the previous test was purged through the tank-engine-exhaust system. The fuel-engine load-emissions control combination was held for several hours on the engine to allow for a sweep of the measurements at varying dilution ratios. Certain dynamometer (e.g., water temperature) and engine (e.g., engine oil temperature) variables were monitored to make sure the engine operation was within the expected range. No special care was taken for engine shutdown.

### 2.1.3 Gas-Phase Measurements

Undiluted tailpipe emissions from the diesel engine were sampled using a Siemens 5-gas analyzer to measure raw concentrations of CO<sub>2</sub>, CO, O<sub>2</sub>, THC (total hydrocarbons) NO and NO<sub>2</sub>. Loss of sample to the tubing walls was avoided through the use of a Teflon<sup>®</sup> line heated to 110 °C. The CO<sub>2</sub> and CO were measured using non-dispersive infrared spectroscopy, the O<sub>2</sub> was measured using a paramagnetic sensor, the THC was measured using a flame ionization detector calibrated with propane, and the NO and NO<sub>2</sub> were measured using chemiluminescence. These measurements were made continuously during an experiment at 1 Hz. A LI-840A (LI-COR Environmental, Nebraska) was used to measure the CO<sub>2</sub> concentrations of the diluted exhaust in the residence tank. The LI-840A when used in this study still maintained its factory calibration. In conjunction with the CO<sub>2</sub> measurements in the undiluted exhaust, the LI-840A measurements allowed for a much more accurate calculation of the dilution ratio than that determined through flow calculations. The dilution ratio was calculated using the following equation:<sup>15</sup>

$$Dilution\ Ratio\ (DR) = \frac{CO_2|undiluted - CO_2|background}{CO_2|diluted - CO_2|background} - (1)$$



where undiluted, diluted, and background concentrations were those measured in the tailpipe, residence tank, and the dilution air respectively.

#### **2.1.4 Particle Collection and Measurements**

*Filter Measurements.* A four-channel filter cart was used to sample diluted particle and vapor emissions from the residence tank. Each channel drew  $16.7 \text{ L min}^{-1}$  (liters per minute) through a  $\text{PM}_{2.5}$  cyclone (URG Corp., North Carolina) and a custom-built filter cartridge – setup to host two filters in series. The cyclone was used to ensure sampling of particles smaller than  $2.5 \text{ }\mu\text{m}$ . The volumetric flow through the cyclone - the value of which controls the particle size cutoff - was set using a mass flow controller controlled using a custom-built LabVIEW software. Temperature- and channel-specific pressure sensors mounted upstream of the filter cartridge but downstream of the cyclone were used to calculate the density of the diluted exhaust (assuming that the exhaust was mostly air and followed the ideal gas law) and to determine the mass flow setpoint that corresponded to a volumetric flow rate of  $16.7 \text{ L-min}^{-1}$  at the cyclone. All calculations and the setpoint operations were performed in the LabVIEW software. Diluted exhaust was drawn into the filter cartridges using a rotary vane vacuum pump (Gast Manufacturing Inc., Michigan). The sampling time for each experiment was adjusted in real time to ensure collection of between 100 and 300  $\mu\text{g}$  of  $\text{PM}_{2.5}$  mass on the filters. Roughly speaking, the sampling times had to be lower (100s of seconds) at the lowest dilution ratio and higher (100s of minutes) at the highest dilution ratio.

Two channels were paired together to collect the particle and vapor sample in the following manner. The first channel contained a front 47-mm Teflon<sup>®</sup> filter to collect particles only and a 47-mm quartz filter behind it to trap semi-volatile vapors (hereafter referred to as the quartz behind Teflon<sup>®</sup> or QBT filter). The second channel contained a front 47-mm quartz filter to

collect all particles and trap semi-volatile vapors (hereafter referred to as the bare quartz or BQ filter) and a 47-mm quartz filter behind it to only trap semi-volatile vapors (hereafter referred to as quartz behind the quartz or QBQ filter). The Teflon<sup>®</sup> filter being hydrophobic is not expected to collect vapors while the quartz filter has been shown to collect vapors with a saturation concentration up to  $10^4 \mu\text{g m}^{-3}$ .<sup>10-12</sup> While the phase (i.e., particle or vapor or particle+vapor) specific collection is expected to work in theory, the actual collection of the different phases on Teflon<sup>®</sup> and quartz filters is much more complicated.<sup>53</sup> For instance, all filters, regardless of the material (e.g., polytetrafluoroethylene or PTFE, and format (e.g., membrane, filter) used, are subject to positive (e.g., adsorption and absorption of vapors onto particle surfaces) and negative artifacts (e.g., evaporation of collected particle species).<sup>54</sup> Nonetheless, the two channel Teflon<sup>®</sup>-quartz arrangement to collect a sample has been widely used in the past to interpret the volatility of primary organic aerosol (POA).<sup>15,54</sup> All filters were 47-mm in size, with the Whatman Teflon<sup>®</sup> filters (7592-104) sourced from GE Healthcare Life Sciences (UK) and the Pallflex quartz filters (2500 QAT-UP) sourced from Pall Corporation (New York).

Prior to use in the filter cartridge, the Teflon<sup>®</sup> filters were stored in 50 mm sterile petri dishes (VWR International, Pennsylvania) and equilibrated for 24 hours in a temperature-controlled room. The quartz filters were prepared for use in the filter cartridges by baking punched filters in a muffle furnace (ThermoFisher Scientific, MA) at 800 °C for seven hours and placed in 50 mm sterile petri dishes after they had cooled to room temperature. From a logistics perspective, only one pair of channels, of the two available, was used for a given experiment while the other pair of channels was prepped for the next experiment. The use of two paired channels helped cut down on sampling and experiment time. At the end of each experiment, petri dishes containing the filter samples were marked with a unique identifier (date-experiment number-filter type-fuel-

engine load-emissions control), sealed with Teflon<sup>®</sup> tape, placed into an experiment-specific ziplock bag, and stored in a freezer at -20 °C.

In addition to the diesel exhaust filter samples, two additional types of measurements were gathered to account for vapors present in the dilution air (dynamic blank) and artifacts introduced through filter handling and storage (handling blank). Since the dilution air was passed through a HEPA filter, there were no particles in the dilution air. In most cases, one dynamic blank was gathered for every day of experiments (a maximum of two experiments were performed in a day) wherein dilution air in the residence tank with the engine turned off was run through the filter cartridges overnight for more than 12 hours. The long sampling times were required to collect enough mass on the filters to perform the gravimetric, composition, and oxidative reactivity measurements described later. Similarly, one handling blank was gathered for every day of experiments. A handling blank was gathered by placing filters into the filter cartridge, waiting for a few minutes, and processing those filters for storage. We conducted a total of 12 dynamic blank experiments and 8 handling blank experiments for our complete study. We collected dynamic blank data for each individual day the engine was running. However, the handling blanks measurements were made for only 8 days only. The number of dynamic and handling blanks measurements were 30% of the total sample measurements data.

*Black Carbon.* A photoacoustic extinctionsmeter (PAX) (Droplet Measurement Technologies, Colorado), connected to the residence tank, was used to measure black carbon (BC) mass concentrations.<sup>55</sup> The PAX used in this study measures BC mass concentrations by measuring the absorbance of laser light at 870 nm.

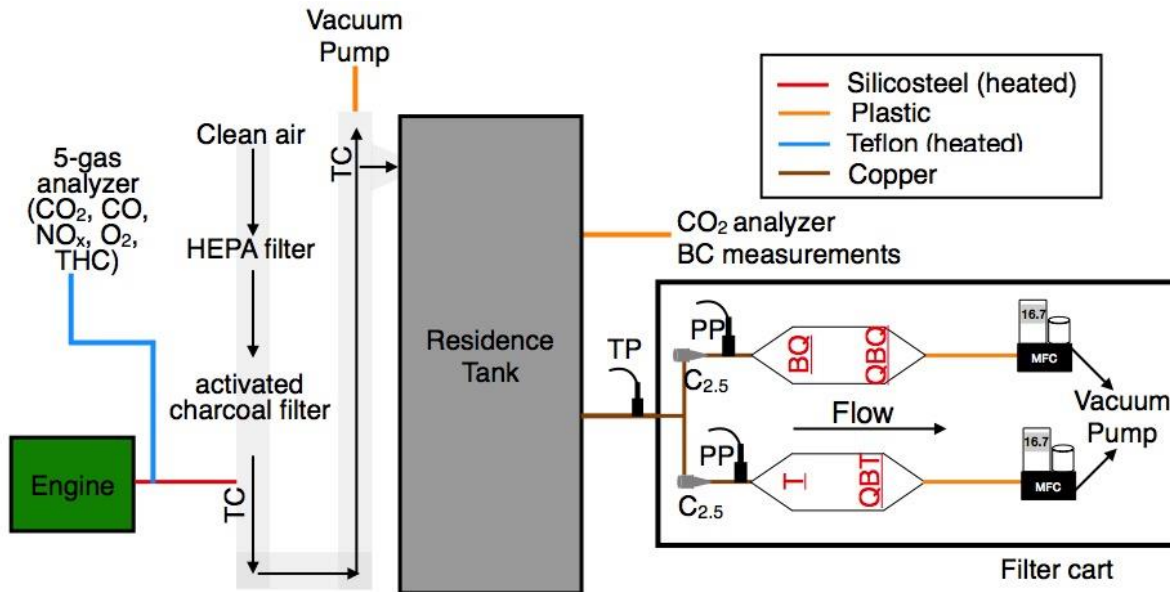


Figure 1: Schematic visualizing the experimental setup and particle collection. MFC = mass flow controller, TC = thermocouple, PP = pressure probe, TP = temperature probe, C<sub>2.5</sub> = PM<sub>2.5</sub> cyclone

## 2.2 Laboratory Measurements and Primary Analysis

A suite of offline techniques were used to analyze the composition and properties of the material collected on the filters. Table 2 describes how the different filter media were consumed, and or not consumed for each laboratory techniques. We collected a total of N=65 samples for fuel-load-emissions control combination and a total of N=20 samples for handling and dynamic blank combinations. The following table describes number of samples analyzed for each laboratory measurements. Given the budget and time sensitivity for this project, we do not use all samples for our analysis.

Table 2: Description and details of the laboratory measurements performed for the various filters collected during the study.

<i>Filter Type</i>	<i>Laboratory Technique and Measurement Performed</i>	<i>Type of Measurement</i>	<i>No. of Samples</i>
Teflon <sup>®</sup>	Gravimetric (PM <sub>2.5</sub> )	Whole/NC	65 out of 65

			samples
	Ion Chromatography (Inorganic Ions)	Whole/C	4 out of 65 samples
	Total Organic Carbon (Water Soluble OC)	Whole/C	4 out of 65 samples
	Transmissometer (BC)	Whole/NC	50 out of 65 samples
	Dithiothreitol Assay (OR)	Whole/C	8 out of 65 samples
Bare Quartz (BQ)	Sunset OC/EC (OC, EC)	Punch/C	65 out of 65 samples
	Dithiothreitol Assay (OR)	Whole/C	22 out of 65 samples
	ICP-MS (Metals)	Punch/C	8 out of 65 samples
Quartz Behind Teflon® (QBT)	Sunset OC/EC (OC, EC)	Punch/C	65 out of 65 samples
	Dithiothreitol Assay (OR)	Whole/C	22 out of 65 samples
Quartz Behind Quartz (QBQ)	Sunset OC/EC (OC, EC)	Punch/C	49 out of 65 samples

*OR=oxidative reactivity, Whole=whole filter was used, Punch=a portion of the filter was cutout for analysis, C=consumed, NC=not Consumed*

### 2.2.1 PM<sub>2.5</sub> Gravimetric Mass

PM<sub>2.5</sub> mass concentrations were calculated based on the particle mass collected on all the Teflon® filters (N=79). Petri dishes containing the Teflon® filters were removed from the freezer and kept in the temperature- and relative humidity-controlled microbalance room for 24 hours to equilibrate to its surroundings. After equilibration and placing the filter on a Polonium radiation strip to remove static charges, three mass measurements were performed on an MX5 microbalance (Mettler Toledo, Switzerland) for each Teflon® sample. The microbalance used for

this study was calibrated every day before start of measurements. A 20,000  $\mu\text{g}$  calibration lab weight and a lab filter (Teflon<sup>®</sup>) with an average filter weight of 14,000  $\mu\text{g}$  (without any mass loading) was used for the calibration. The data were recorded and observed for any measurement deviation. There were no such deviations observed during the course of this study. The average of the three measurements was recorded in units of  $\mu\text{g}$ . The average mass flow rate in standard cubic meters per minute recorded by the mass flow controller in the LabVIEW software was multiplied by the sampling time in minutes to calculate the total volume of air at STP (standard temperature and pressure) conditions in units of  $\text{m}^3$ . The mass and volume were used to calculate the  $\text{PM}_{2.5}$  mass concentration in units of  $\mu\text{g m}^{-3}$ . All raw gravimetric  $\text{PM}_{2.5}$  masses were corrected for mass collected on the Teflon<sup>®</sup> filters during handling and storage using the median value obtained from the handling blanks (handling artifact=7.7  $\mu\text{g}$ , N=5) and all gravimetric  $\text{PM}_{2.5}$  mass concentrations were corrected for vapor collection on Teflon<sup>®</sup> filters with the median value obtained from the dynamic blanks (dynamic artifact=2.7  $\mu\text{g m}^{-3}$ , N=9). Note that the dynamic blank filters also had to be corrected for handling and storage artifacts.

### **2.2.2 Organic and Elemental Carbon**

The organic (or primary organic aerosol) and elemental carbon (OC/POA and EC) fractions of  $\text{PM}_{2.5}$  were measured using the field (or semi-continuous) version of the Sunset OC/EC analyzer (Sunset Laboratory Inc., Oregon) following the NIOSH 5040 method.<sup>56</sup> All BQ (N=85) and QBT (N=85) filters were analyzed for OC and EC but only a fraction of the QBQ filters (N=62) were analyzed for OC and EC since that data was only used for diagnostic purposes (e.g., determining breakthrough of EC particles, studying vapor artifacts behind a quartz filter). Briefly, a 2.27  $\text{cm}^2$  punch from a quartz filter is placed into the analyzer. Carbon in the sample is determined by thermal-optical transmission (TOT)<sup>57</sup> and a non-dispersive infrared detector is

used to measure the total carbon evolved during thermal desorption from the filter as carbon dioxide. OC is determined first in a helium environment, while EC is determined second in a helium/oxygen environment. The transmission through the filter is monitored to correct for any OC that is pyrolyzed to EC during the thermal desorption process. The Sunset OC/EC was calibrated for OC using a sucrose standard stock solution (10  $\mu\text{g C}$ ). The OC and EC masses measured by the instrument data acquisition system ( $\mu\text{g C}$ ) were divided by the punch surface area (2.27  $\text{cm}^2$ ), multiplied by the active surface area of the filter (12.01  $\text{cm}^2$ ), and divided by the sampled mass of air at STP conditions to calculate OC and EC mass concentrations in units of  $\mu\text{g C m}^{-3}$ .

### **2.2.3 Inorganic and Water-Soluble OC**

The inorganic and water-soluble OC (WSOC) particles on a handful of Teflon<sup>®</sup> filters (N=4) were measured using ion chromatography. We selected one filter each for one of the Diesel-Idle-None, Diesel-Load-None, Biodiesel-Idle-None, and Biodiesel-Load-None experiments. We did not analyze any filters from the DPF+DOC experiments. For each sample, particles on the Teflon<sup>®</sup> filter were extracted into 15 ml of deionized (DI) water in a Nalgene Amber HDPE (high-density polyethylene) bottle by sonicating without heat for 40 minutes. The extracts were filtered to ensure that the insoluble particles were removed using a 0.2  $\mu\text{m}$  PTFE (polytetrafluoroethylene) syringe filter. The water-soluble ions were measured using a dual channel Dionex ICS-3000 ion chromatography system. Each channel includes a pump, self-regenerating anion or cation SRS-ULTRA suppressor, and conductivity detector. The inorganic cations were separated using a Dionex IonPac CS12A analytical column (3 $\times$ 150 mm) with an eluent of 20 mM methanesulfonic acid at a flow rate of 0.5  $\text{ml min}^{-1}$ . A Dionex IonPac AS14A analytical (4 $\times$ 250 mm) column employing an eluent of 1 mM sodium bicarbonate/8 mM sodium

carbonate at a flow rate of  $1 \text{ ml min}^{-1}$  was used for the inorganic anion analysis. The injection volume and analysis time for both methods was  $50 \text{ }\mu\text{L}$  and 17 minutes, respectively. Each channel was calibrated using eight multi-compound standards in order to create calibration curves. The WSOC concentration of each liquid extract was determined using a Sievers Model 800 Turbo Total Organic Carbon (TOC) Analyzer. The analyzer converts the organic carbon in the sample to carbon dioxide by employing chemical oxidation via reaction with ultraviolet light and ammonium persulfate. The carbon dioxide formed is measured by conductivity. The increase in the observed conductivity is proportional to the amount of organic carbon in the sample. When measuring the liquid extracts the analyzer was run in Turbo mode to provide a 3 second integrated measurement. The TOC Analyzer was factory calibrated and the calibration was periodically verified by injection of oxalic acid standards. The masses measured by the instrument data acquisition system in  $\mu\text{g}$  were divided by the sampled mass of air at STP conditions to calculate mass concentrations of sulfate, nitrate, ammonium, chloride, and WSOC in units of  $\mu\text{g m}^{-3}$ . This analysis was performed by Dr. Amy Sullivan at Atmospheric Sciences at the Foothills Campus of CSU.

#### **2.2.4 Trace Metals**

A handful of BQ filters ( $N=10$ ) and QBT filters ( $N=2$ ) were analyzed using Inductively Coupled Plasma Mass Spectrometry (ICP-MS) to determine the mass concentrations of copper (Cu), manganese (Mn), zinc (Zn), iron (Fe), vanadium (V), nickel (Ni), lead (Pb), and cobalt (Co). We selected one filter each for one of the Diesel-Idle-None, Diesel-Load-None, Biodiesel-Idle-None, and Biodiesel-Load-None experiments. We did not analyze any filters from the DPF+DOC experiments. Briefly, small square sections of the quartz filter were cut using a ceramic scissor instead of a conventional metal punch to avoid contaminating the ICP-MS sample. A high-



resolution photograph of the remaining quartz filter was used and the GIMP open-source software was used to determine the coordinates of the punch. A google Excel spreadsheet was used to perform the calculation and following the surface area of the ICP-MS sample was determined. The ICP-MS filter sample was placed in a 50 ml extraction tube containing 20 ml of 3.5% HNO<sub>3</sub> spiked with 50 ppb of Galium (Ga), Indium (In), and Bismuth (Bi), that were used as internal standards. The extraction tube was heated to and kept at 95 °C for one hour and allowed to cool for 30 minutes, before diluting with deionized water to create a 50 ml liquid sample. The liquid sample was vortexed for 10 seconds, allowed to stand for at least 30 minutes, shaken again, and finally allowed to settle for an hour. The liquid sample was run through an ELAN ICP-MS (PerkinElmer Inc., Massachusetts) where the solution was nebulized into a high temperature argon plasma to produce ionized gaseous elements that were detected in a mass spectrometer.<sup>58</sup> Each sample solution was analyzed three times and the average of the three measurements was recorded. The ICP-MS was calibrated using a laboratory prepared multi-element stock solution prior to its use in this work. The raw mass measurements in µg, corrected for with the internal standard data, were divided by the cutout surface area, multiplied by the active surface area of the filter (12.01 cm<sup>2</sup>), and divided by the sampled mass of air at STP conditions to calculate trace metal mass concentrations in units of µg m<sup>-3</sup>. This analysis was performed by Dr. Jacqueline M. Chaparro at the Proteomics and Metabolomics Facility at CSU.

### **2.2.5 Dithiothreitol Assay**

A fraction of the Teflon<sup>®</sup> (N=10 out of 81), BQ (N=31 out of 85), and QBT (N=22 out of 85) filters were used to perform a dithiothreitol (DTT) assay to quantify the oxidative reactivity of DEPs. We selected four co-measured Teflon<sup>®</sup>, BQ, and QBT filters from each of the Diesel-Idle-None, Diesel-Load-None, Biodiesel-Idle-None, and Biodiesel-Load-None experiments and two

paired BQ and QBT filters from the Diesel-Load-DPF+DOC experiments. Filters for the DTT assay were chosen from experiments conducted at higher dilution ratios (average dilution ratio of 103.2 for the non-DPF+DOC experiments and average dilution ratio of 7.8 for the DPF+DOC experiments) to ensure atmospherically relevant particle concentrations but at the same time chosen to ensure that there was sufficient mass collected on the filter to perform the DTT assay. We also selected two co-measured Teflon<sup>®</sup>, BQ, and QBT filters from each of the dynamic blank and handling blank experiments. The following paragraphs describe how we performed the sample extraction and DTT assay and how those measurements were used to calculate the oxidative reactivity.

Table 3: Details of the DTT assay performed in this work resolved by experiment type (fuel-engine load-emissions control combination), filter media, solvent used for extraction, and treatment of the extract (filtered versus unfiltered).

<i>Fuel-load-emissions control</i>	<i>Water based solvent (Phosphate Buffer)</i>				<i>Organic solvent (DCM)</i>			
	<i>Particles+Vapors (BQ)</i>		<i>Vapors (QBT)</i>	<i>Teflon<sup>®</sup> Membrane</i>		<i>Particles+vapors (BQ)</i>		<i>Vapors (QBT)</i>
	<i>Filtered</i>	<i>Unfiltered</i>		<i>Filtered</i>	<i>Unfiltered</i>	<i>Filtered</i>	<i>Unfiltered</i>	
Diesel-Idle-None	4	4	4	2	2	1	1	1
Diesel-Load-None	4	4	4	2	2	1	1	1
Biodiesel-Idle-None	4	4	4	2	2	1	1	1
Biodiesel-Load-None	4	4	4	2	2	1	1	1
Diesel-Idle-DPF+DOC	-	-	-	-	-	-	-	-
Diesel-Load-DPF+DOC	2	2	2	-	-	-	-	-
Handling Blank	-	3	-	-	1	-	1	-
Dynamic Blank	-	4	-	-	1	-	1	-
Total sample filters	25		18	10		6		4

*BQ=bare quartz, QBT=quartz behind Teflon<sup>®</sup>, DCM=dichloromethane, DPF=diesel particulate filter, DOC=diesel oxidation catalyst*

*Sample Extraction.* The sample filter (N=10 out of the 10 Teflon<sup>®</sup> and N=43 out of the 53 quartz) was placed in an 8 or 20 ml Nalgene Amber HDPE bottle and filled with 0.1 M of phosphate buffer solution. The phosphate buffer solution was a 50:50 mixture of high purity potassium phosphate dibasic and potassium phosphate monobasic, adjusted to a pH of 7.4 (matched to the pH of human blood), and cleaned for transition metals using a chelating agent (Chelex<sup>®</sup> 100 sodium form).<sup>37</sup> The phosphate buffer solution was prepared and consumed within a few weeks to reduce the possibility of contamination. For the quartz filters, the volume of the buffer solution added to the Nalgene bottle was adjusted between 3 to 15 ml to ensure a concentration of 25 to 40  $\mu\text{g ml}^{-1}$  of  $\text{PM}_{2.5}$  in solution. The concentration range was selected based on a few measurements performed on test samples that best matched the dynamic range of the DTT assay.<sup>59,60</sup> For the Teflon<sup>®</sup> filters, the buffer solution volume was kept constant at 15 ml. A larger volume of the buffer solution was used with the Teflon<sup>®</sup> filter since the polypropylene support ring on the filter made it hard to keep the filter fully immersed in the buffer solution when we used a volume of 6 ml. The Nalgene bottles were sonicated at 37 °C for 75 minutes and later cooled to ambient temperature over 2 hours. Most prior work that has used a water-based solvent to extract  $\text{PM}_{2.5}$  has used deionized water for the extraction step and then mixed an aliquot of the extract into a phosphate buffer solution to prepare for the DTT assay. In our work, doing so would have resulted in additional dilution of the  $\text{PM}_{2.5}$  and produced a weaker concentration of  $\text{PM}_{2.5}$  in the phosphate buffer solution and deviated from our target  $\text{PM}_{2.5}$ -in-solution concentration. We do not know if our extraction method directly into the phosphate

buffer solution introduced an experimental artifact and this may need to be explored in future work.

McWhinney et al.<sup>35</sup> found that the filterable material in DEPs (e.g., black carbon) accounted for a large fraction of the observed oxidative reactivity. To test that hypothesis, half of the PM<sub>2.5</sub> extract was filtered using a 2 µm filter (PTFE syringe filter) and the DTT assay was performed separately on the unfiltered and filtered extracts. The filtration was performed only on the PM extracted from the Teflon<sup>®</sup> and BQ filters as the QBT filters had very little particle mass to perform both an unfiltered and filtered test. Several studies have suggested that hydrophobic particles, particularly those found in fresh emissions, may be more readily extracted with the use of an organic solvent when compared to a water-based solvent.<sup>37,61,62</sup> To test the DTT assay response to extraction with an organic solvent, a handful of the BQ filters (N=6 out of 53) were placed in an 8 ml Nalgene bottle, filled with 6 ml of HPLC (high-performance liquid chromatography) grade dichloromethane (DCM), and sonicated at room temperature for 15 minutes. Unlike extraction with the phosphate buffer solution, these filters were not sonicated at 37 °C because DCM has a boiling point of 39.6°C at 1 atm. So that the DTT assay was performed identically for all the filter sample solutions, a rotary evaporator (Buchi, Netherlands) was used to evaporate the dichloromethane under vacuum. The rotary evaporator was run at 150 RPM (revolutions per minute) for approximately 40 minutes until all the DCM was evaporated. The particles in the Nalgene bottle, presumably stuck to the walls of the vial, were reconstituted in phosphate buffer solution and the process described earlier was repeated.

*DTT Assay.* The DTT assay was performed identically for all sample solutions regardless of the filter type or organic solvent used during the extraction process. 500 µl of sample solution (PM<sub>2.5</sub> in phosphate buffer solution) was drawn from the Nalgene bottle used for the extraction and was

mixed with 15  $\mu\text{l}$  of 0.0045 M DTT solution in a 1.5 ml centrifuge tube (Eppendorf, Germany) and shaken to initiate the DTT reaction with  $\text{PM}_{2.5}$ . After shaking, the vial was placed in a water bath held at 37 °C. 100  $\mu\text{l}$  aliquots were removed from the vial every 15 minutes (i.e., at 0, 15, 30, and 45 minutes) and added to 400  $\mu\text{l}$  of 50  $\mu\text{M}$  DTNB solution to react the remaining DTT with DTNB to form TNB. TNB absorbs light at 412 nm and the absorbance at that wavelength was measured either using an Agilent 8453 or Varian Cary 100 Bio UV-vis spectrophotometer (both by Agilent Technologies, CA) to determine the concentration of TNB and by association the molar concentration of DTT; one molecule of DTT reacts with one molecule of DTNB to form two molecules of TNB solution. The change in the DTT concentration with time was fit assuming a linear model to calculate the DTT decay in units of  $\mu\text{M min}^{-1}$ . The raw DTT decay was normalized by the  $\text{PM}_{2.5}$  concentration in solution to determine the oxidative reactivity in units of  $\text{nmoles min}^{-1} \mu\text{g PM}^{-1}$ . The oxidative reactivity measurements in the literature are very often described in these units. All oxidative reactivity measurements were corrected for laboratory blanks that were performed on the phosphate buffer solution as well for handling and dynamic blanks collected during the experiments.

### **2.2.6 SootScan Black Carbon**

In addition to the PAX, BC was measured from the sample collected on a Teflon<sup>®</sup> filter using a SootScan Optical Transmissometer Model OT21 (Magee Scientific; Berkeley, CA). The transmissometer measures the difference in the amount of light attenuated through a reference filter and a filter loaded with  $\text{PM}_{2.5}$ . The measurements were performed using the 880 nm wavelength channel and corrected for the loading effect.<sup>63</sup> Based on earlier work with DEPs,<sup>63,64</sup> we used an attenuation coefficient of  $16.6 \text{ m}^2\text{g}^{-1}$ . Instrument attenuation performance was checked before the start of experiment with referenced Neutral density optical glass discs

(provided by Magee scientific) with stable absorbance. The instrument performance was unchanged and was within limits of errors from the date of manufacture. All SootScan BC data (N=49) was corrected for handling and dynamic blanks (N=14).

### 2.3 Secondary Analysis

*Emission Factors.* Emission factors of the gas- and particle-phase pollutants were calculated to compare emissions at different fuel, engine load, and emissions control combinations and to facilitate comparison with values in the literature. The emission factors in units of g kg-fuel<sup>-1</sup> were calculated using equation 3:

$$EF_X = \frac{\Delta X}{\Delta CO_2} \times \frac{MW_{CO_2}}{MW_C} \times C_f \times 10^3 \quad (2)$$

Where  $\Delta X$  and  $\Delta CO_2$  are the background-corrected pollutant and  $CO_2$  concentrations in  $\mu\text{g m}^{-3}$  respectively,  $MW_{CO_2}$  (44 g mole<sup>-1</sup>) and  $MW_C$  (12 g mole<sup>-1</sup>) are the molecular weights for  $CO_2$  and carbon, and  $C_f$  is the mass fraction of carbon in the fuel. According to Gordon et al.,<sup>65</sup>  $C_f$  was assumed to be 0.85 g kg-fuel<sup>-1</sup> for diesel and 0.77 g kg-fuel<sup>-1</sup> for biodiesel. This formulation for the emission factor calculation assumes that all of the carbon in the fuel was released as  $CO_2$ .

*POA Volatility.* The POA volatility or the partitioning of POA between the gas and particle phases was assessed using two different methods. In the first method, we used the positive artifact from vapor adsorption on the bare quartz (BQ) and quartz behind Teflon<sup>®</sup> (QBT) filters. This technique has been used extensively in the past<sup>9-12,66</sup> and was recently validated for diesel exhaust POA against three independent techniques.<sup>12</sup> Briefly, for the same primary emissions from the engine, varying the dilution ratio produces different concentrations in the residence tank and perturbs the gas/particle equilibrium of POA. A lower dilution ratio results in a larger fraction in the particle phase and a lower fraction in the gas phase and vice versa. When

sampling, the BQ filter is expected to trap both POA and semi-volatile gases in equilibrium with it while the QBT filter is expected to trap only the semi-volatile gases since the POA is filtered on the Teflon<sup>®</sup> filter upstream of the QBT filter. As a larger fraction of the semi-volatile gases+POA material is moved to the gas-phase with an increasing dilution ratio, the QBT filter traps an increasingly larger fraction of the total material relative to the BQ filter. This shift in the material from the BQ to QBT filter can be used to infer POA volatility. In previous work, the fraction of POA in the particle phase ( $X_p$ ) expressed against the POA mass concentration has been used as a measure of the POA volatility. Following May et al.,<sup>11</sup>  $X_p$  is calculated using equation 4:

$$X_p = \frac{OC_{BQ} - OC_{QBT}}{OC_{BQ}} \quad (3)$$

Where  $OC_{BQ}$  and  $OC_{QBT}$  are the OC mass concentrations in units of  $\mu\text{g m}^{-3}$  on the BQ and QBT filters respectively. Previous work has used this partitioning behavior to determine the volatility distribution of POA that reflects the distribution of vapor pressures of the organic compounds that constitute POA. This volatility distribution can be described with the volatility basis set (VBS) framework using a set of semi-volatile surrogate species that are logarithmically spaced in volatility or saturation concentration space.<sup>67</sup> The following equations describe the gas/particle partitioning of POA:

$$\xi_i = \left(1 + \frac{C_i^*}{POA}\right)^{-1} \quad (4)$$

$$POA = \sum \alpha_i C_{total} \xi_i \quad (5)$$

Where  $\xi_i$  is the fraction of the organic mass in bin  $i$  that is in the particle phase,  $C_i^*$  is the effective saturation concentration for bin  $i$  in  $\mu\text{g m}^{-3}$  at 300 K, POA is the POA mass

concentration in  $\mu\text{g m}^{-3}$ ,  $\alpha_i$  is the fraction of the total (gas+particle) mass in bin  $i$ , and  $C_{total}$  is the total (gas+particle) mass in  $\mu\text{g m}^{-3}$ . For a predefined  $C^*$  set of  $[1^0 10^1 10^2 10^3 10^4] \mu\text{g m}^{-3}$ , the gas/particle partitioning data were fit to determine an  $\alpha$  set that represented the POA volatility distribution.

*Oxidative Reactivity Factors.* The oxidative reactivity measurements in units of  $\text{nmoles min}^{-1} \mu\text{g PM}^{-1}$  were used to calculate an oxidative reactivity factor in units of  $\text{nmoles min}^{-1} \text{kg-fuel}^{-1}$  and  $\text{nmoles min}^{-1} \text{kWh}^{-1}$  to investigate the cumulative effect from burning a unit mass of fuel or unit amount of energy produced respectively. This was done by multiplying the oxidative reactivity measurement in units of  $\text{nmoles min}^{-1} \mu\text{g PM}^{-1}$  by the emission factor for  $\text{PM}_{2.5}$  in units of  $\mu\text{g kg-fuel}^{-1}$  or  $\mu\text{g kWh}^{-1}$ . Since the oxidative reactivity measurements used in this analysis were performed on the quartz filter, we could not use the  $\text{PM}_{2.5}$  emission factor calculated based on the Teflon<sup>®</sup> filter. The emission factor for  $\text{PM}_{2.5}$  for the quartz filter was determined by multiplying the emission factor for OC by an organic matter-to-organic carbon ratio of 1.2<sup>11,68</sup> and adding the emission factor for EC.



### 3 Results

#### 3.1 Emission Factors for Gaseous Pollutants

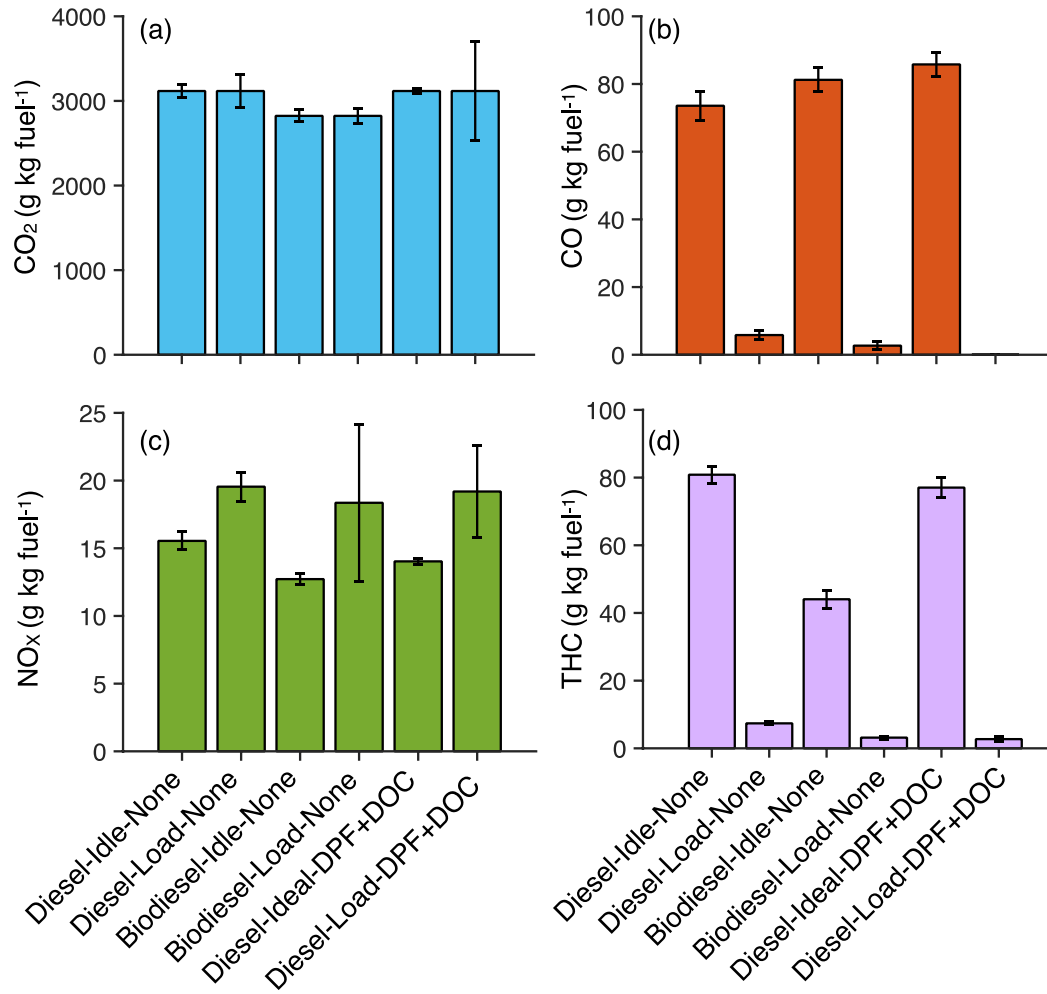


Figure 2: Emission factors for (a) CO<sub>2</sub>, (b) CO, (c) NO<sub>x</sub> and (d) THC for the various fuel-engine load-emissions control combinations in units of g kg-fuel<sup>-1</sup>.

In Figure 2 we observe the emission factors for CO<sub>2</sub>, CO, NO<sub>x</sub> and THC for the various fuel-engine load-emissions control combinations in units of g kg-fuel<sup>-1</sup>. The bars and the error bars represent the distribution of the emission factors from multiple experiments performed for the

same fuel-engine load-emissions control combination. Emissions of CO<sub>2</sub>, within the measurement uncertainty, were the same with the diesel fuel with and without the emissions control. Compared to diesel, the CO<sub>2</sub> emissions were ~10% lower for biodiesel possibly on account of a lower carbon mass fraction in biodiesel. The diesel or biodiesel fuels were not analyzed for their carbon mass fraction in this work but typical differences for the carbon mass fraction for diesel (~0.85 g kg-fuel<sup>-1</sup>) and soy-based biodiesel (~0.77 g kg-fuel<sup>-1</sup>) would account for the findings presented here.<sup>65</sup> Average CO and THC emissions were significantly higher at the idle load condition (74-86 g kg-fuel<sup>-1</sup> of CO and 44-81 g kg-fuel<sup>-1</sup> of THC) than at the 50% load condition (~0-6 g kg-fuel<sup>-1</sup> of CO and 3-7 g kg-fuel<sup>-1</sup> of THC) with and without the emissions control system on because the engine had a lower combustion efficiency at idle loads. In contrast, the average NO<sub>x</sub> emissions did not seem to vary much between the different combinations but were slightly higher at the 50% load (20-30%) than at idle load, presumably from higher engine temperatures that facilitate NO<sub>x</sub> production at higher loads. The use of biodiesel had mixed effects on the emissions of CO, THC, and NO<sub>x</sub> when compared to those from diesel. Average CO emissions with biodiesel were higher at idle load (10%) but lower at 50% load (45%) when contrasted against those from diesel. Average THC and NO<sub>x</sub> emissions on the other hand were lower for biodiesel when compared to diesel fuel for both idle (46% for THC and 18% of NO<sub>x</sub>) and 50% load (57% for THC and 6% of NO<sub>x</sub>) conditions. The NO<sub>x</sub> reductions with biodiesel were surprising since a majority of prior studies have found NO<sub>x</sub> emissions to increase with the use of biodiesel.<sup>69</sup> The use of an emissions control system (DPF+DOC) seemed to slightly increase or decrease the CO and THC emissions at idle load but had a larger impact at 50% load where CO and THC emissions were reduced by a factor of 3.74 and 2.7 respectively. The relatively small changes at the idle load but larger differences at the

50% load suggests that the emissions control system may be limited at idle loads where the catalyst temperatures might be lower than the light off temperatures for effective oxidation of CO and THC. Our group made the same finding with this engine in a previous study.<sup>45</sup> At the 50% load condition with and without the emissions control for the diesel fuel, emissions of CO (5.8 g kg-fuel<sup>-1</sup> and 0.016 g kg-fuel<sup>-1</sup> respectively) met the non-road Tier-3 and Tier-4 emissions standard of ~20.8 g kg-fuel<sup>-1</sup> of CO. However, at the 50% load condition, emissions of THC+NO<sub>x</sub> without the emissions control (27 g kg-fuel<sup>-1</sup>) and emissions of THC with the emissions control (2.7 g kg-fuel<sup>-1</sup>) did not meet the Tier 3 (~16.7 g kg-fuel<sup>-1</sup> of THC+NO<sub>x</sub>) or interim non-road Tier 4 (~0.8 g kg-fuel<sup>-1</sup> of THC) emissions standards respectively. This might be because the emissions control was retrofitted to the exhaust system without recalibrating the engine.

### **3.2 Emission Factors for Particle Pollutants**

In Figure 3, we plot the emission factors for PM<sub>2.5</sub>, POA, and EC and the EC/OC ratios for all the data measured in this study. To remind the reader, the PM<sub>2.5</sub> data are from the gravimetric Teflon<sup>®</sup> filter measurements while the POA and EC data are from the quartz filter measurements. The POA data were corrected for positive artifacts. Median emissions of PM<sub>2.5</sub>, POA, and EC were higher at the idle condition when compared to the 50% load condition from more incomplete combustion at lower loads. With the exception of a few outliers (circled in magenta), median emissions of PM<sub>2.5</sub>, POA, and EC with the emissions control device were one to two orders of magnitude lower than without the emissions control device. These reductions agree well with previously observed reductions with the use of a diesel particle filter, which is expected to reduce particle emissions by 95% or more. When compared to diesel, biodiesel use resulted in lower median emissions of PM<sub>2.5</sub> and POA at the idle condition (43% lower for PM<sub>2.5</sub>

and 33% lower for POA) but had higher emissions at the 50% load condition (17% higher for PM<sub>2.5</sub> and 45% higher for POA). In contrast, with biodiesel use, median EC emissions were 62% lower for the idle condition and 83% lower for the 50% load condition. The lower EC emissions with biodiesel meant that the POA:EC ratios were generally lower for biodiesel compared to diesel. At the 50% load condition, the PM<sub>2.5</sub>, POA, and EC emission factor range for diesel use with and without the emissions control compared modestly with recent emission factors compiled by May et al.<sup>70</sup> from a range of source and near-road studies, suggesting that the engine and its operation were representative of in-use engines and engine technology; see Table 4.

Table 4: Emission factors for CO, THC, NO<sub>x</sub>, PM<sub>2.5</sub>, POA, and EC compared against the 25<sup>th</sup>-75<sup>th</sup> percentile data compiled in May et al.<sup>70</sup> from a range of dynamometer<sup>71-74</sup>, on-road<sup>75,76</sup>, and tunnel studies<sup>77-79</sup>.

<i>Species</i>	<i>This work: Diesel-Load-None</i>	<i>This work: Diesel-Load-DPF+DOC</i>	<i>Non-DPF Diesels (May et al., 2014)</i>	<i>DPF Diesels (May et al., 2014)</i>
CO (g kg fuel <sup>-1</sup> )	2-9.8	0-0.3	3-11	0.01-6
THC (g kg fuel <sup>-1</sup> )	6-8.7	0.5-4.9	0.4-1.5	0-0.1
NO <sub>x</sub> (g kg fuel <sup>-1</sup> )	16.4-22.7	9-29.3	5-13	2-10.5
PM <sub>2.5</sub> (g kg fuel <sup>-1</sup> )	0.15-0.3	0.003-0.009	0.450-0.650	0.002-0.005
POA (g kg fuel <sup>-1</sup> )	0.15-0.3	0.0019-0.0086	0.06-0.09	0.003-0.007
EC (g kg fuel <sup>-1</sup> )	0.09-0.13	0.0003-0.0022	0.18-0.2	0-0.0008

### 3.3 PM<sub>2.5</sub> Composition and Closure

Emission factors for the carbonaceous species (POA and EC), inorganic ions, and metals are tabulated in Table 4. We should note that while the emission factors for the carbonaceous species have been calculated for all the experiments, the emission factors for the inorganic ions and metals have been calculated on a small subset of the experiments and hence cannot be directly compared against the carbonaceous species. Nonetheless, emission factors for the inorganic ions

and metals can be qualitatively compared to the carbonaceous species to examine general trends in the PM<sub>2.5</sub> composition. Across the four fuel-engine load combinations, POA and EC accounted for most of the PM<sub>2.5</sub> mass with the inorganic ions and metals accounting for approximately 5% and 1% of the PM<sub>2.5</sub> mass respectively. Nitrite and nitrate accounted for about half, followed by calcium that accounted for a quarter, of the inorganic ion mass. Emissions of sulfate for the diesel fuel were low presumably from the use of ultra-low sulfur diesel (ULSD) and even lower for biodiesel as there is very little sulfur for fuel derived from plant feedstocks.<sup>80</sup> Overall, Cu and Fe accounted for the most (~75%) of the trace metal mass followed by Zn, Mn, and Pb. The Pb emissions factor seemed higher for diesel fuel and it possibly could be from lube oil in the engine. The ICP-MS analysis was unable to detect any vanadium, cobalt, or nickel. Overall, the use of biodiesel fuel resulted in lower emissions for the carbonaceous, inorganic, and metal species compared to the diesel fuel.

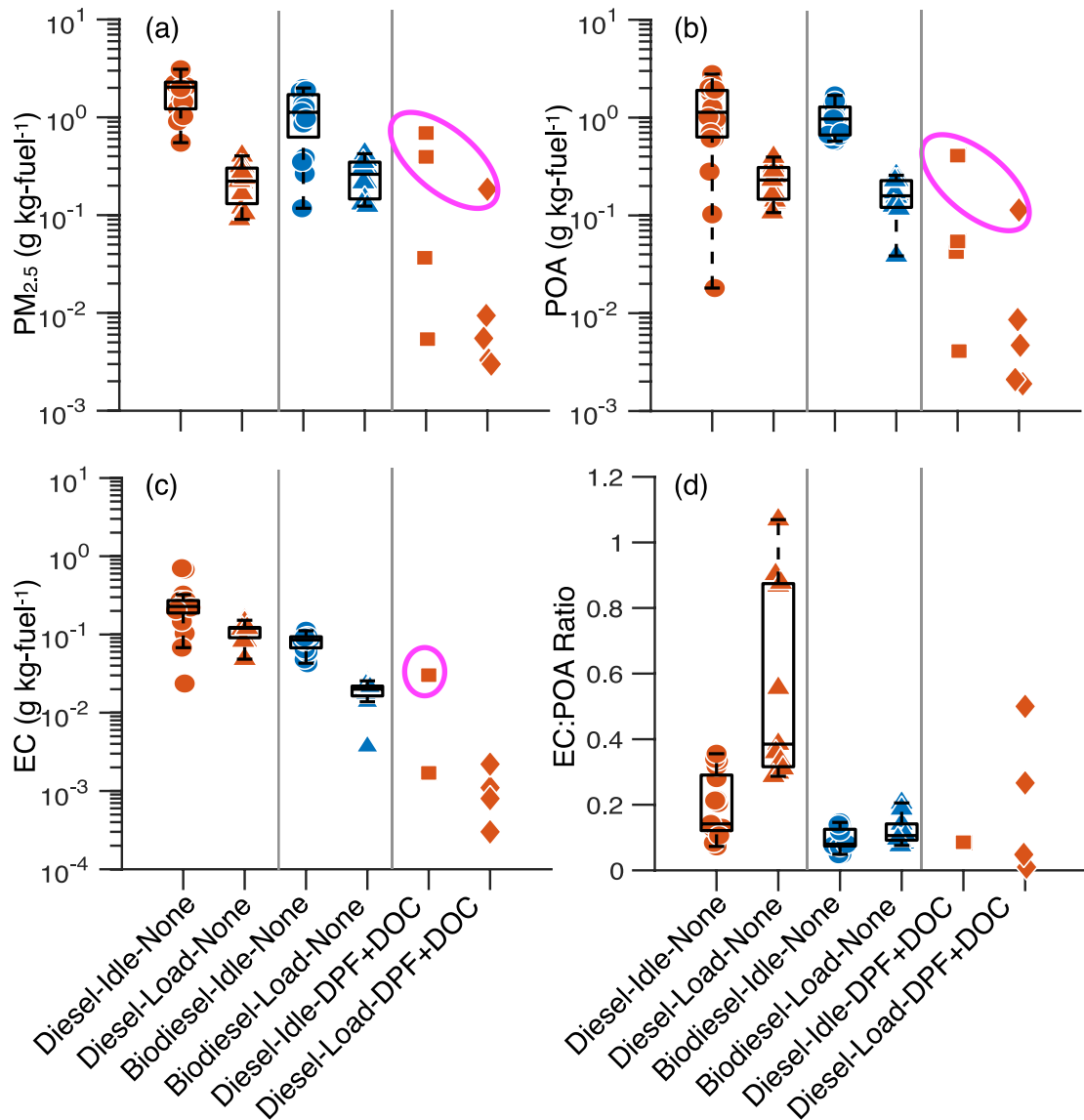


Figure 3: Emission factors for (a)  $PM_{2.5}$ , (b) POA, and (c) EC in units of  $g\ kg\text{-fuel}^{-1}$  and the (d) EC:POA ratio for the various fuel-engine load-emissions control combinations. Panels include both the box plot and the individual data used to create the box plot. The box presents the 25<sup>th</sup>, 50<sup>th</sup>, and 75<sup>th</sup> percentile of the data and the whiskers present the lowest and highest values that are not outliers. Outliers are defined as points that lie three times beyond the interquartile range. Outliers in the DPF+DOC data are circled in magenta. Values less than zero are not shown.

Table 5: Emission factors for POA, EC, inorganic compounds, and trace metals for all fuel-engine load combinations without emissions control. The inorganic ions and metals were not measured for the experiments with emissions control.

Type	Species	Diesel-Idle-None	Diesel-Load-None	Biodiesel-Idle-None	Biodiesel-Load-None
Carbon (g kg-fuel <sup>-1</sup> )	POA	1.22±0.616 (N=19)	0.232±0.08 8 (N=11)	0.903±0.332 (N=16)	0.160±0.050 (N=10)
	EC	0.229±0.117 (N=19)	0.111±0.03 4 (N=11)	0.076±0.041 (N=16)	0.018±0.007 (N=10)
Inorganic <sup>#</sup> (mg kg-fuel <sup>-1</sup> )	Sulfate (SO <sub>4</sub> )	7.83	14.65	2.85	0.73
	Nitrate (NO <sub>3</sub> )	14.20	7.30	7.65	3.76
	Nitrite (NO <sub>2</sub> )	26.90	23.14	14.45	2.05
	Ammonium (NH <sub>4</sub> )	1.91	1.04	1.09	0.57
	Cl	0.25	0.31	BDL	BDL
	Ca	28.83	9.41	12.95	2.08
	Na	ND	Outlier	0.53	0.06
	Mg	4.51	0.97	0.33	0.12
	K	5.06	5.75	0.96	0.51
Metals <sup>&amp;</sup> (mg kg-fuel <sup>-1</sup> )	Cu	9.90	5.17	2.99	0.21
	Fe	8.51	3.08	0.01	0.71
	Mn	3.33	1.46	0.57	~0
	Zn	0.64	0.37	0.77	0.47
	Pb	1.15	0.32	0.06	0.04

BDL=below detection limit, ND=no data, <sup>#</sup>=results from a single quartz filter sample, <sup>&</sup>=averaged results from two BQ filter samples

As POA and EC accounted for the most of the PM<sub>2.5</sub> mass, we expected the PM<sub>2.5</sub> mass gathered on the Teflon<sup>®</sup> filter to agree with the sum of the artifact corrected POA and EC measured on the

BQ filter. In Figure 4, we plot the sum of the POA and EC mass concentrations against the  $PM_{2.5}$  mass concentrations. The comparison showed significant variability in achieving mass closure between the POA+EC and  $PM_{2.5}$  values, with 58% and 82% of the data lying within a factor of 2 and 3 respectively. On average, the POA+EC mass concentrations were biased low compared to the  $PM_{2.5}$  mass concentrations with a mean normalized bias of -18.8% and mean normalized error of 84.3%. Consistent with our finding, May et al.<sup>70</sup> tested three medium and heavy-duty diesel vehicles without a DPF and found that the POA+EC mass concentrations were about half of the  $PM_{2.5}$  mass concentrations. The POA+EC mass concentrations were possibly lower than the  $PM_{2.5}$  values because we used a lower POA:OC ratio (1.2 based on the work of Lipsky and Robinson<sup>15</sup> and Aiken et al.<sup>81</sup>) or and/or we overcorrected for the artifact on the BQ filter.

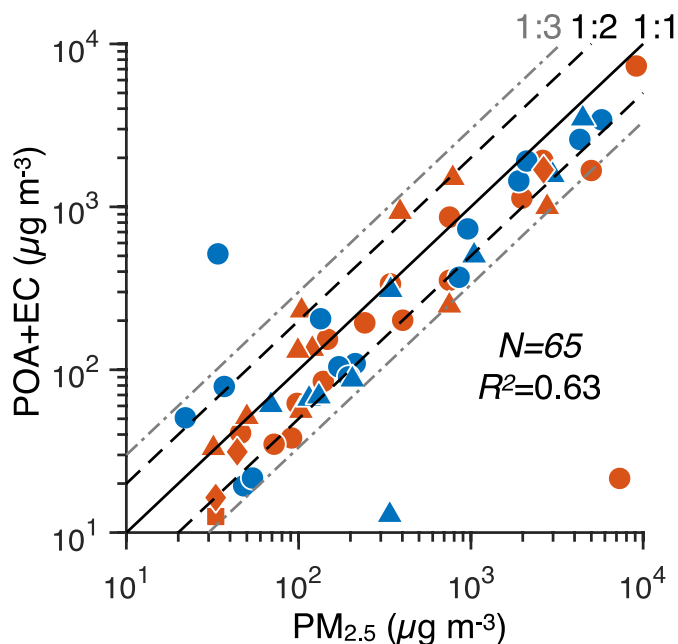
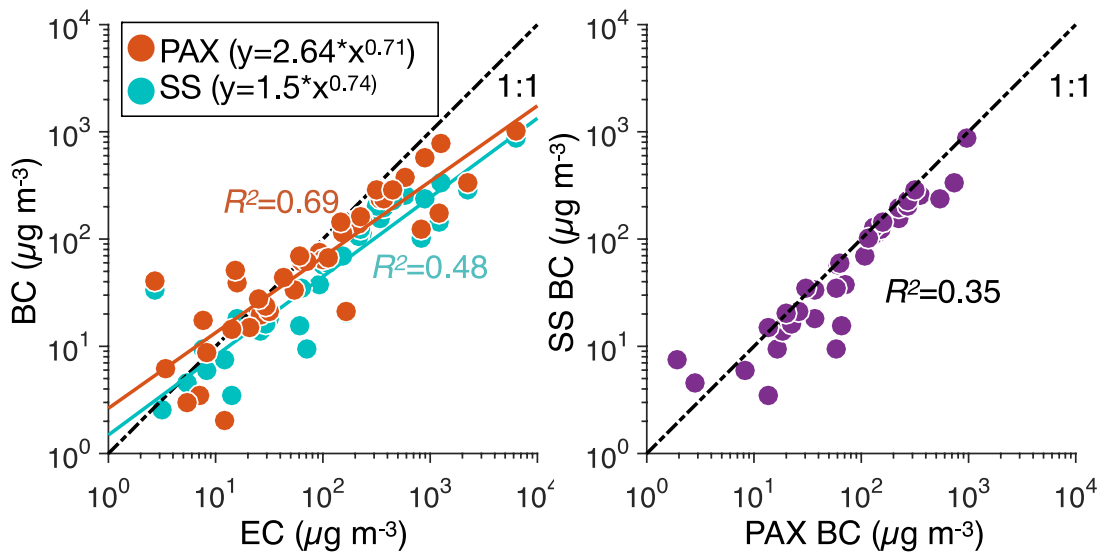


Figure 4: Scatter plot comparing the measured mass concentrations of POA+EC against mass concentrations of  $PM_{2.5}$  for all experiments performed in this work. The POA data have been artifact corrected.



We used three different methods to measure soot emissions from the engine and these measurements were compared against each other in Figure 5(a-b). To reiterate, the EC was measured with a thermo-optical technique using the Sunset OC/EC analyzer. The BC was measured in two different ways: (i) using a SootScan that measures the attenuation of light through particles collected on a Teflon<sup>®</sup> filter and (ii) using a PAX that measures the absorption in an aerosol sample in real time. We found that the BC correlated well with EC ( $R^2=0.78$  for PAX and  $R^2=0.82$  for SootScan) but both measurements of BC were biased low compared to EC, particularly at the higher concentrations. For example, at an EC mass concentration of  $100 \mu\text{g m}^{-3}$ , the PAX BC mass concentration was only  $69 \mu\text{g m}^{-3}$  and the SootScan BC mass concentration was  $45 \mu\text{g m}^{-3}$ , based on the fits developed in Figure 5(a). The two BC measurements agreed more with each other (see Figure 5(b)) than with the EC measurements. The EC mass concentrations may be higher than the BC mass concentrations for reasons ranging from protocol-related artifacts in the Sunset OC/EC<sup>82,83</sup> to assumptions about the mass absorption cross-section used in the PAX and SootScan.



*Figure 5: (a) Scatter plot comparing mass concentrations of BC measured by the SootScan (SS) and PAX against mass concentrations of EC measured by the Sunset OC/EC analyzer for all experiments performed in this work. (b) Scatter plot comparing mass concentrations of BC measured by the SootScan (SS) against those measured by the PAX for all experiments performed in this work.*

### **3.4 POA Volatility**

The changes in the gas/particle partitioning of POA or the POA volatility are visualized by plotting the fraction of POA mass in the particle phase ( $X_p$ ) against the POA mass concentration in Figure 6. Across all experiments,  $X_p$  decreased with a decreasing POA suggesting that the POA mass evaporated as the POA mass concentration was decreased with increasing dilution. Interestingly, we did not observe significant differences in the POA volatility between the different fuel, engine load, and emissions control combinations. Biodiesel POA at both the idle and load conditions appeared to have a slightly lower volatility (or higher  $X_p$ ) for POA at the higher POA mass concentrations. Overall, the partitioning trends implied that while the POA emissions may have varied much more across the different combinations (see Figure 3), the POA volatility was similar. The similar POA volatility offers advantages in modeling POA emissions in atmospheric models as the same volatility distribution could be used to represent vehicle emissions operated with different fuels and emissions control configurations.

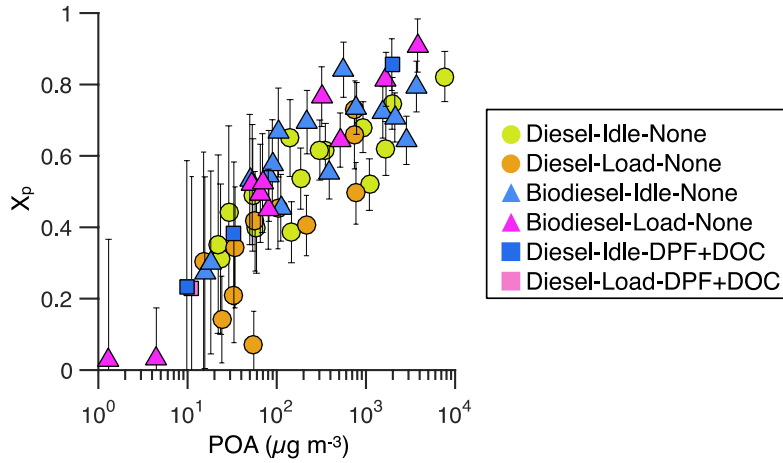


Figure 6: Fraction of POA mass in the particle phase ( $X_p$ ) plotted against the POA mass concentrations for all experiments performed in this work.

As the POA volatility did not appear to change with fuel, engine load, or emissions control, we used the data in Figure 6 to develop a volatility distribution fit that represented the POA volatility. The volatility distribution – set of  $\alpha$ 's as defined in equation (5) – were determined in Matlab using the non-linear fitting function, 'nlinfit'. As the ambient and sample temperatures varied slightly between the different experiments ( $15.9 \pm 3.7$  °C) and that the  $C^*$ s were predefined at 27 °C or 300 K, we accounted for changes in the  $C^*$  with temperature using the Clausius-Clapeyron equation:

$$C^*(T) = C^*(300 \text{ K}) \exp\left(\frac{\Delta H_{vap}}{R} \left(\frac{1}{300} - \frac{1}{T}\right)\right) - (6)$$

Where  $\Delta H_{vap}$  is the enthalpy of vaporization in  $\text{kJ mole}^{-1}$ ,  $R$  is the universal gas constant ( $8.314 \text{ kJ mole}^{-1} \text{ K}^{-1}$ ), and  $T$  is the temperature in K. The enthalpy of vaporization for use in the Clausius-Clapeyron equation was based on the work of Epstein et al.:<sup>84</sup>

$$\Delta H_{vap} = -11 \log_{10} C^* + 131 - (7)$$

The volatility distribution that best fit the data was  $\alpha=[0.0813 \ 0.5657 \ 0.2508]$  for  $C^*=[1 \ 100 \ 10000] \mu\text{g m}^{-3}$ . Note that the values of  $\alpha$  sum to 1. The POA volatility predicted by the fits along with the 25<sup>th</sup> to 75<sup>th</sup> percentile confidence intervals is compared against the raw measurements in Figure 7(a). The predicted POA volatility was lower than most of the measurements because the volatility distribution was tied to a  $C^*$  set predefined at a higher temperature (27 °C) while the POA samples were gathered at slightly cooler temperatures ( $15.9\pm 3.7$  °C). For a more appropriate comparison, the predictions of  $X_p$  for the corresponding temperatures were compared to measurements of  $X_p$  in Figure 7(b). Predictions were within 50% of the measurements for more than 90% of the data.

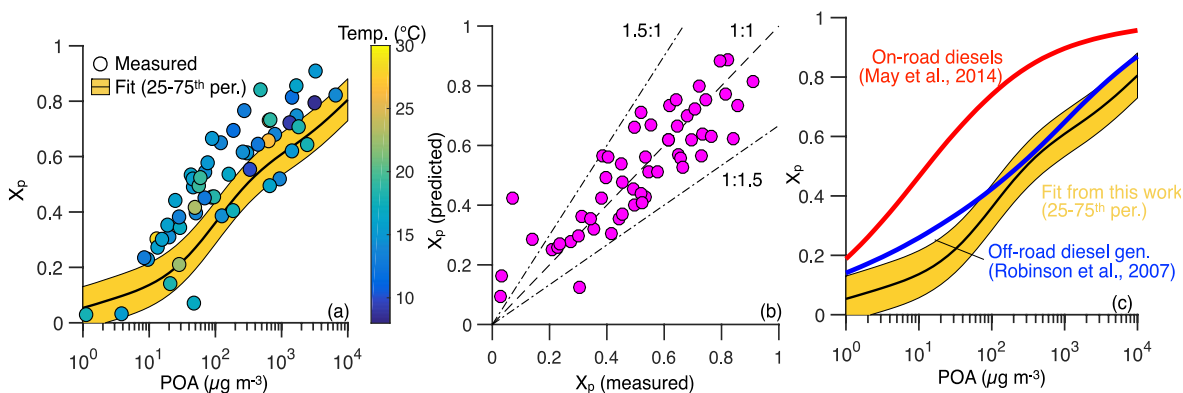


*Figure 7: Fraction of POA mass in the particle phase ( $X_p$ ) plotted against the POA mass concentrations for all experiments performed in this work. Panel (a) compares raw measurements against estimates based on the volatility distribution fits. Panel (b) compares estimates of  $X_p$  based on the volatility distribution fits against measurements using a scatter plot. Panel (c) compares predictions of  $X_p$  against those estimated by earlier work.*

The predicted POA volatility was also compared to the volatility previously estimated by Robinson et al.<sup>9</sup> for POA from a small off-road diesel generator and May et al.<sup>11</sup> for POA from a suite of on-road medium- and heavy-duty diesel vehicles. Robinson et al.<sup>9</sup> and May et al.<sup>11</sup> used similar methods to determine the volatility and hence the results from this work should be

directly comparable. The POA volatility from this work compared better with that from the small off-road diesel generator but was more volatile than that from the on-road vehicles, suggesting that on- and off-road vehicle POA may need to be modeled separately in atmospheric models.

### **3.5 Oxidative Reactivity**

In this section, we first examine differences in the oxidative reactivity of DEPs for the engine variables explored in this work, namely fuel, engine load, and emissions control. The oxidative reactivity of DEPs is presumably a strong function of DEP composition and hence we later examine how differences in the PM composition, extraction methods, and filter media contribute to/modify the oxidative reactivity.

#### **3.5.1 Fuel and Engine Load Effects**

Results from the oxidative reactivity measurements performed on the BQ filters for experiments run without the emissions control are presented in Figure 8. To remind the reader, the BQ filter trapped all particles and semi-volatile vapors and hence the DTT assay performed on the BQ filter quantified the oxidative reactivity for particles and vapors together. The influence of fuel on the oxidative reactivity is captured in panels (a) and (b) while the influence of load is captured in panels (c) and (d). The data in panels (a) and (b) are the same as the data in panels (c) and (d), just reorganized. Solid lines connecting the medians of the distributions were overlaid on the data to show gross trends. Finally, an unpaired 2 sample *t*-test was performed with the data to determine statistical significance across the dimension of interest. A *p*-value smaller than 0.05 was considered significant.

As shown in Figure 8(a), on a  $\mu\text{g}$  PM basis, biodiesel use resulted in a lower oxidative reactivity than diesel at both load conditions. For biodiesel, this median oxidative reactivity was 68% lower at idle conditions and 93% lower at load conditions than diesel. As biodiesel use mostly

produced lower PM<sub>2.5</sub>, POA, and EC emissions at both engine loads (see Section 3.2 for more details), the oxidative reactivity on a kg-fuel basis, as shown in Figure 8(b), was even lower for biodiesel when compared to diesel. For biodiesel, this median oxidative reactivity was 83% lower at the idle condition and 97% lower at the load condition than diesel. It appears that that use of biodiesel – at least that derived from soy – in a diesel engine when run without the emissions control significantly reduces the DTT-based oxidative reactivity of DEPs. Our finding is consistent with some but not all earlier DTT-DEP work. For example, Kooter et al.<sup>34</sup> measured the oxidative reactivity of DEPs from a Euro III heavy-duty diesel engine run on biodiesel (likely from soy) and found a 95% reduction in the oxidative reactivity compared to diesel when expressed on an emission factor basis ( $\mu\text{moles min}^{-1} \text{kWh}^{-1}$ ). Gerlofs-Nijland et al.<sup>85</sup> measured the oxidative reactivity of DEPs from a Euro 4 diesel passenger vehicle without a DPF run on a 50:50 blend of diesel:biodiesel (rape seed). For an urban driving cycle, they observed that the use of a biodiesel blend compared to diesel resulted in an ~85 and ~90% reduction in the oxidative reactivity when expressed on a  $\mu\text{g PM}$  basis ( $\text{nmoles min}^{-1} \mu\text{g PM}^{-1}$ ) and emission factor basis ( $\text{nmoles min}^{-1} \text{km}^{-1}$ ) respectively. However, the oxidative reactivity with the biodiesel blend appeared to be similar or higher when the vehicle was operated on a rural (or highway) driving cycle when compared to diesel. Holmen et al.<sup>86</sup> ran an industrial light-duty diesel engine and measured the oxidative reactivity of DEPs for varying blends of biodiesel derived from soy and waste vegetable oil with diesel. They found that the oxidative reactivity on a  $\mu\text{g PM}$  basis decreased by 50-80% with an increased biodiesel proportion although the reduction in oxidative reactivity was dependent on the biodiesel feedstock. Fukagawa et al.<sup>87</sup> and Grigoratos et al.<sup>88</sup> compared the oxidative reactivity of DEPs from modern diesel vehicles run on diesel and biodiesel:diesel blends. In contrast to our findings, they found that the biodiesel blends produced

an increase in the oxidative reactivity compared to diesel when expressed on a  $\mu\text{g PM}$  basis; a 42% increase for the study of Fukagawa et al.<sup>87</sup> and a 14-21% increase for the study of Grigoratos et al.<sup>88</sup> It is possible that the inconsistencies in the fuel effect between the different studies could be attributed to differences in biodiesel quality and feedstock and the use of diesel-biodiesel blends rather than the use of neat biodiesel. This may need to be examined in more detail in future DTT studies focused on effects of fuel on the oxidative reactivity of DEPs.

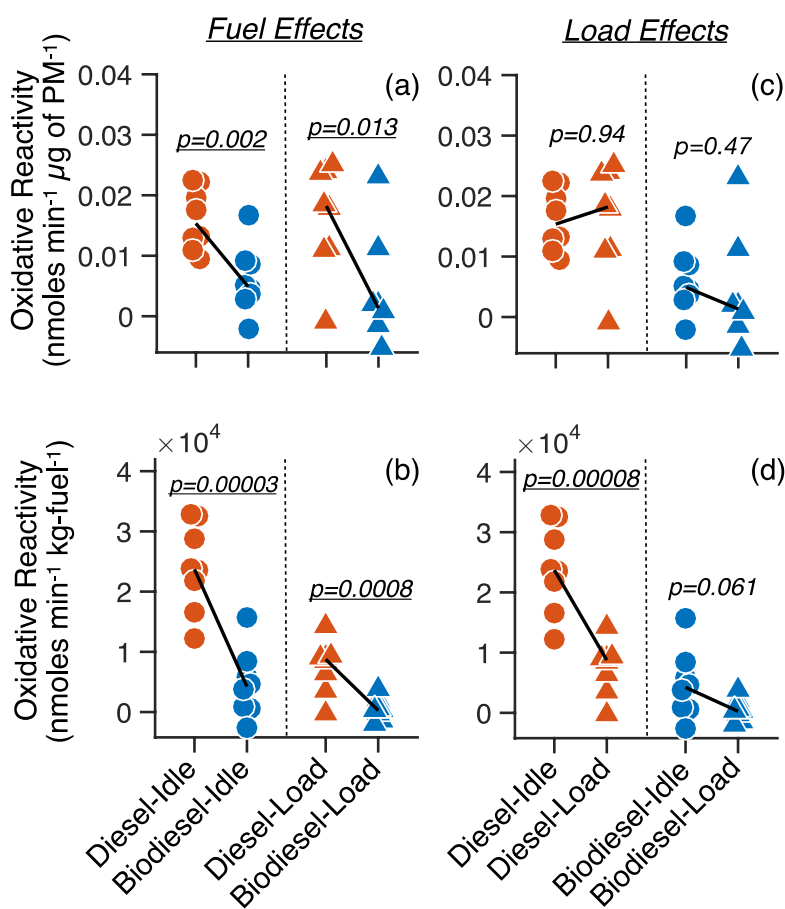


Figure 8: Measured oxidative reactivity of DEPs in two different units (a,c)  $\text{nmoles min}^{-1} \mu\text{g PM}^{-1}$  and (b,d)  $\text{nmoles min}^{-1} \text{kg-fuel}^{-1}$ . The presented data are resolved by fuel (diesel=orange, biodiesel=blue) and engine load (idle=circle, load=triangle). Panels (a) and (b) capture fuel effects while panels (c) and (d) capture load effects. The black solid line connects the medians of

*the distributions that are compared and p-values are shown in italic with significant p-values underlined.*

The oxidative reactivity on a  $\mu\text{g}$  PM basis, as shown in Figure 8(c), was approximately the same between the two different engine loads regardless of the fuel used, suggesting that engine load may not be an important modifier for the oxidative reactivity of DEPs. Unlike the fuel effect, our finding contradicted at least one other DTT-based study and two non-DTT based studies that examined the load effect. McWhinney et al.<sup>35</sup> performed oxidative reactivity measurements on DEPs from an engine from a Tier 1 light-duty diesel vehicle and found that the oxidative reactivity of DEPs when expressed on a  $\mu\text{g}$  PM basis generally increased with engine load. They attributed the increase in oxidative reactivity to higher proportion of EC in  $\text{PM}_{2.5}$  at higher loads; we test this hypothesis with our data later. Betha et al.<sup>89</sup> measured the oxidative reactivity of DEPs from a small diesel generator using a glutathione assay and observed that a higher engine load produced a doubling in oxidative reactivity on  $\mu\text{g}$  PM basis for biodiesel derived from waste cooking oil but did not see the same effect for diesel. Pourkhesalian et al.<sup>90</sup> used a pro-fluorescent nitroxide molecular probe to measure the oxidative reactivity of DEPs from a Euro III diesel engine. They observed that the oxidative reactivity of DEPs when expressed on a  $\mu\text{g}$  PM basis decreased by  $\sim 97\%$  as the engine load was ramped from idle to full load and they hypothesized that the higher oxidative reactivity at lower loads stemmed from incomplete combustion of lubricating oil contributing to PM emissions. On a kg-fuel basis, however, the oxidative reactivity, as shown in Figure 8(b), was higher at idle conditions than at load conditions on account of higher PM emissions at idle than at load conditions, although this effect for biodiesel was not suggestive given our low sample size ( $N=8$ ) ( $p=0.061$ ).



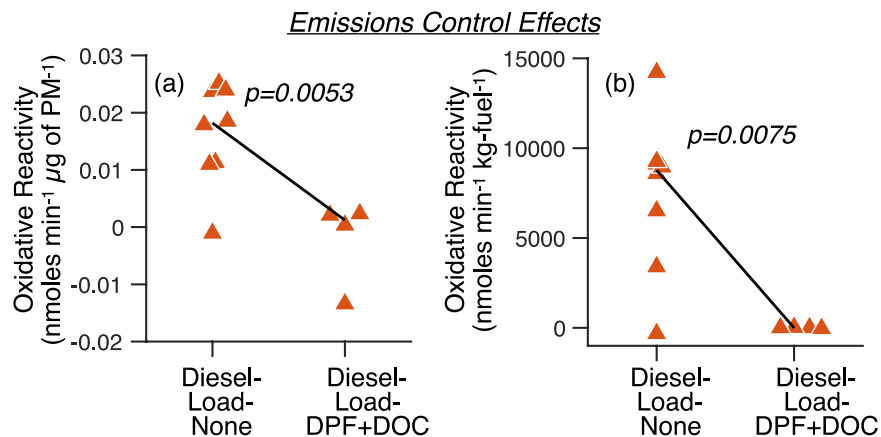


Figure 9: Measured oxidative reactivity of DEPs comparing experiments with and without the emissions control in two different units (a)  $\text{nmoles min}^{-1} \mu\text{g PM}^{-1}$  and (b)  $\text{nmoles min}^{-1} \text{kg-fuel}^{-1}$ . The black solid line connects the medians of the distributions that are compared and  $p$ -values are shown in italic with significant  $p$ -values underlined.

### 3.5.2 Emissions Control Effects

Results from the oxidative reactivity measurements performed on the BQ filters for experiments run with diesel fuel at 50% load condition and with and without the emissions control are presented in Figure 9. To reiterate, the emissions control system consisted of a diesel oxidation catalyst (DOC) that oxidized CO and unburned hydrocarbons to  $\text{CO}_2$  and a diesel particle filter (DPF) that trapped particles. On a  $\mu\text{g PM}$  basis, as shown in Figure 9(a), the emissions control resulted in a significantly lower oxidative reactivity for DEPs that on median was 93% lower than without the emissions control. This suggested that the emissions control was effective in removing particle (and/or vapor) species that contributed to the oxidative reactivity. Since the emissions control also resulted in substantial decreases in the  $\text{PM}_{2.5}$ , POA and EC emissions (see Section 3.2 for more details), the oxidative reactivity on a  $\text{kg-fuel}$  basis, as shown in Figure 9(b), was mostly lower with the emissions control on. The median oxidative reactivity with the

emissions control was at least three orders of magnitude lower than without the emissions control.

The finding, again, agrees with some but not all earlier studies that have performed DTT-based measurements to examine the influence of emissions control on the oxidative reactivity of DEPs. For example, Kooter et al.<sup>34</sup> found that the oxidative reactivity for DEPs from a Euro III heavy-duty diesel engine were more than 95% lower on a  $\mu\text{g}$  PM basis with the use of a DPF. Similarly, Grigoratos et al.<sup>88</sup> observed a three- to six-fold decrease in oxidative reactivity on an emission factor basis that they attributed to oxidation of organic compounds in the DOC. In contrast, Biswas et al.<sup>32</sup> found the oxidative reactivity of DEPs to vary with emissions control technology where in some instances the oxidative reactivity on a  $\mu\text{g}$  PM basis was higher (e.g., factor of  $\sim 8$  for an uncatalyzed DPF) but in other cases lower (e.g., half for a catalyzed DPF) than without the use of any emissions control technology. On a rural driving cycle, which is comparable to the load condition used in this work, Gerlofs-Nijland et al.<sup>85</sup> found that the oxidative reactivity of DEPs on a  $\mu\text{g}$  PM basis increased by more than an order of magnitude with the use of a DPF. Regardless of the differences in the oxidative reactivity of DEPs across studies on a  $\mu\text{g}$  PM basis, the dramatic reduction in  $\text{PM}_{2.5}$  mass with the use of an emissions control device meant that all studies consistently observed a reduced oxidative reactivity with the use of emissions control technologies.

### **3.5.3 Understanding Links to $\text{PM}_{2.5}$ Composition**

The  $\text{PM}_{2.5}$  composition should be a strong predictor of oxidative reactivity and we examined correlations between the carbonaceous components of DEPs (i.e., black and organic carbon) measured in  $\text{g kg-fuel}^{-1}$  and the oxidative reactivity measured in  $\text{nmoles min}^{-1} \text{kg-fuel}^{-1}$ . Linear regressions of the oxidative reactivity against (a)  $\text{PM}_{2.5}$ , (b) EC, and (c,d,e) different phases of

OC are plotted in Figure 10 on an emission factor basis. The oxidative reactivity had the poorest correlation with  $PM_{2.5}$  ( $R^2=0.05$ ) and the strongest correlation with EC ( $R^2=0.78$ ). Amongst the three variants of OC, the oxidative reactivity showed the strongest correlation with vapors measured on the QBT filter although the correlation was not as strong as that for EC. Both EC and semi-volatile vapors have previously been found to correlate with oxidative reactivity and the paragraphs below discuss our attempts to link  $PM_{2.5}$  composition to oxidative reactivity.

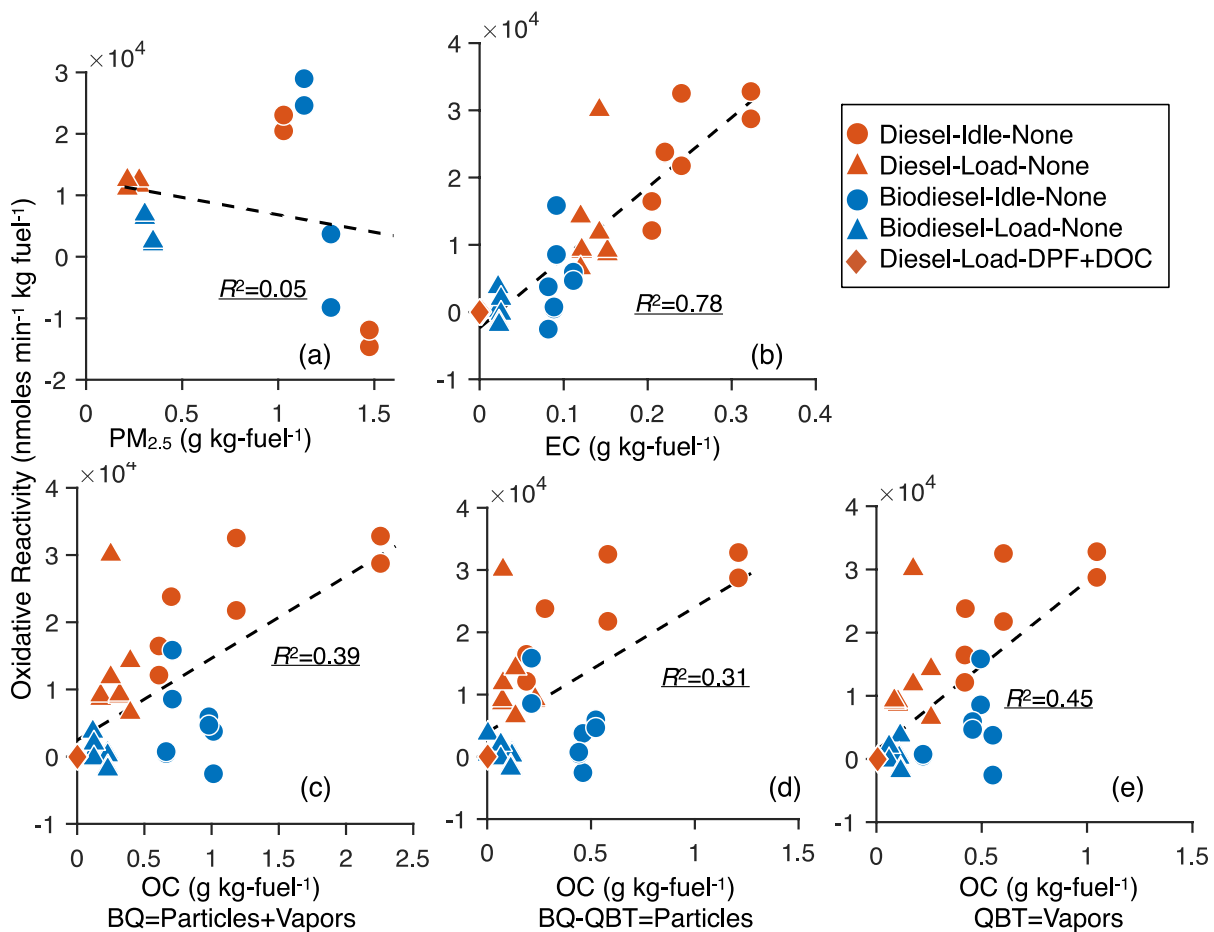


Figure 10: Measured oxidative reactivity of DEPs in  $nmol\ min^{-1}\ kg\ fuel^{-1}$  regressed against emission factors for (a)  $PM_{2.5}$ , (b) EC, (c) particle+vapor OC, (d) particle OC, and (e) vapor OC. The dashed lines are linear fits to the data.

The strong correlation with EC was consistent with the conclusions of McWhinney et al.<sup>35</sup> who found that the oxidative reactivity of DEPs on a  $\mu\text{g PM}$  basis increased at higher loads from an increased proportion of EC in  $\text{PM}_{2.5}$ . The oxidative reactivity of DEPs on a  $\mu\text{g PM}$  basis in McWhinney et al.<sup>35</sup> was a factor of 1.5 to 4.5 higher than the median oxidative reactivity measured in our work but the differences in the absolute measurements of the oxidative reactivity between the two studies could be attributed to the different proportions of EC and POA in  $\text{PM}_{2.5}$ . The diesel engine used by McWhinney et al.<sup>35</sup> produced a higher EC:POA ratio (0.6-3.3) than the diesel engine used in this work (0.06-0.7). In contrast, Biswas et al.<sup>32</sup> found oxidative reactivity to correlate poorly with EC but that might have been because the Biswas et al.<sup>32</sup> study mostly focused on DEPs from varying emissions control technologies while our oxidative reactivity-EC correlations were derived from data mostly gathered without any emissions control. The DTT assays performed on the unfiltered and filtered extracts prepared from the BQ filters were used to assess the influence of EC on the oxidative reactivity of DEPs. EC should not dissolve in the phosphate buffer solution during PM extraction and hence the oxidative reactivity measurements performed on the filtered extract should not be affected by EC. The raw oxidative reactivity measurements performed on the unfiltered and filtered extracts are compared in Figure 11. Surprisingly, on aggregate, the oxidative reactivity measurement was very similar between the two extracts implying that the filtration had a small to no influence on the measurement. It is unclear why the oxidative reactivity correlated so strongly with EC but that the filtered extract, which should be devoid of EC, produced the same result as the unfiltered extract. One way in which this confounding result can be explained is that the species responsible for the oxidative reactivity are correlated with EC but are also soluble in water. One such class of compounds, called quinones (oxygenated aromatic compounds), has been shown to

be reactive towards DTT and previously measured in DEPs<sup>82</sup>. We did not measure quinones in our study but would recommend that they be studied in future DEP-oxidative reactivity efforts.

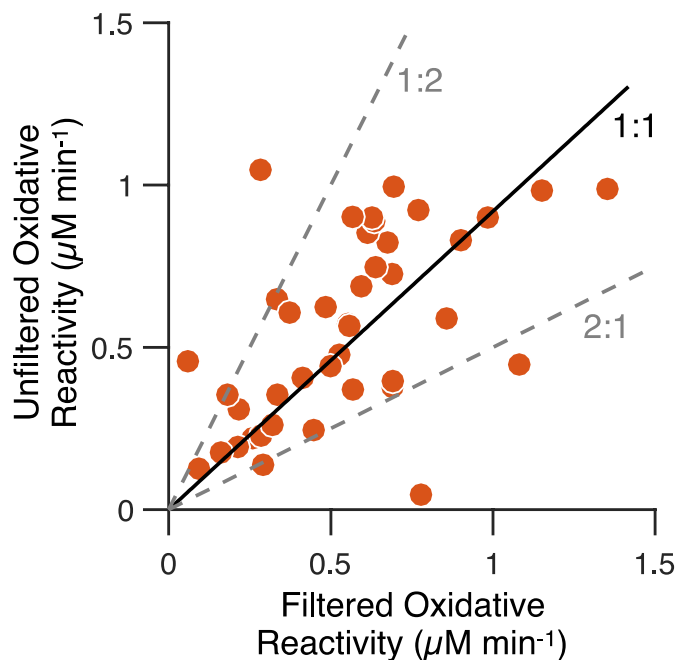


Figure 11: Scatter plot of the raw oxidative reactivity measurements in  $\mu\text{M min}^{-1}$  performed on unfiltered and filtered extracts prepared from all BQ filters.

Our correlation with semi-volatile vapors was consistent with findings from Biswas et al.<sup>32</sup>. Biswas et al.<sup>32</sup> measured differences in the oxidative reactivity of bare and thermally denuded (at 150 and 230 °C) DEPs and inferred that the semi-volatile fraction of OC in DEPs contributed substantially to the oxidative reactivity. We arrived at the same qualitative conclusion in this work by examining the oxidative reactivity of the semi-volatile vapors trapped on the backup quartz filter (see Figure 10(e)) although our correlations do not state the contribution of semi-volatile vapors to the oxidative reactivity. We further probed the influence of semi-volatile

vapors by comparing the oxidative reactivity of vapors (collected on QBT filters) to that of particles+vapors (collected on BQ filters) for the different fuel and engine load combinations run without the emissions control. These results are plotted in Figure 12. The oxidative

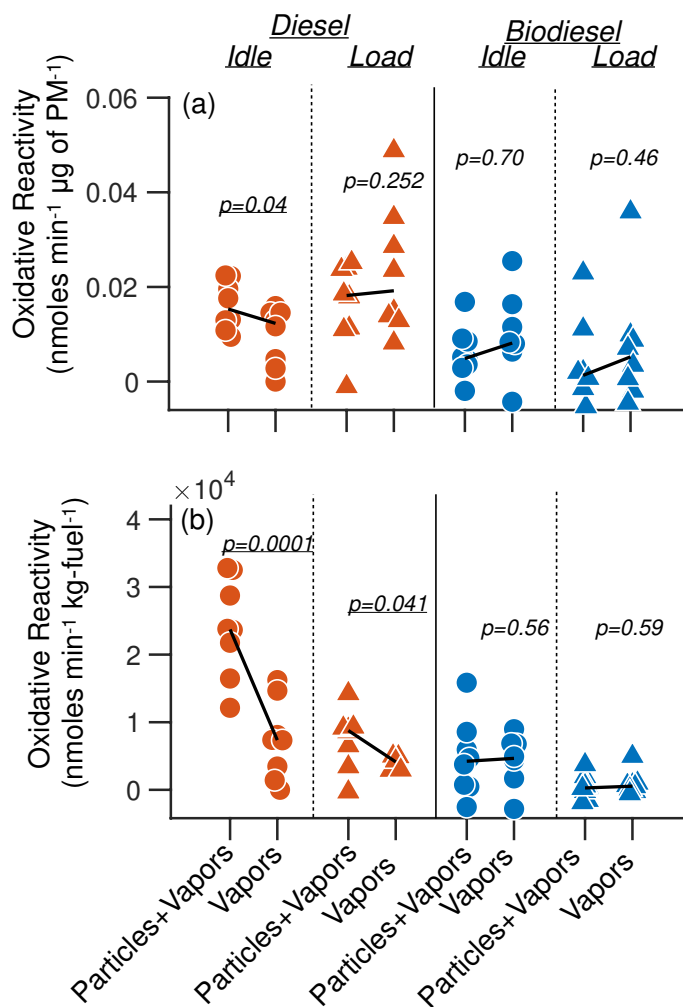


Figure 12: Measured oxidative reactivity of DEPs resolved by phase of the material (particles+vapors and vapors) in two different units (a)  $\text{nmoles min}^{-1} \mu\text{g PM}^{-1}$  and (b)  $\text{nmoles min}^{-1} \text{kg-fuel}^{-1}$ . The presented data are resolved by fuel (diesel=orange, biodiesel=blue) and engine load (idle=circle, load=triangle). The black solid line connects the medians of the distributions that are compared and  $p$ -values are shown in italic with significant  $p$ -values underlined.

reactivity on a  $\mu\text{g PM}$  basis, as shown in Figure 12(a), did not appear to vary between the particles+vapors and vapors for any of the fuel (i.e., diesel, biodiesel) and load (i.e., idle, load) combinations, suggesting that the particles and vapors had roughly the same oxidative reactivity. However, as the mass emissions of particles+vapors were larger than those for the vapors alone, the oxidative reactivity on a kg-fuel basis was larger for particles+vapors compared to the vapors, for diesel fuel at both load conditions. We did not observe the same effect for biodiesel because the mass emissions of particles+vapors, with significantly reduced EC emissions (see Figure 3(c)), were similar to those for vapors. To estimate the contribution of semi-volatile vapors to the oxidative reactivity measured for the particles+vapors, we compare the raw oxidative reactivity measurements in  $\mu\text{M min}^{-1}$  for all paired BQ (particles+vapors) and QBT (vapors) filters in Figure 13. While there is substantial scatter, the slope of the linear fit suggests that the semi-volatile vapors collected on the QBT filters could probably account for about a quarter of the oxidative reactivity of the particles+vapors collected on the BQ filters.

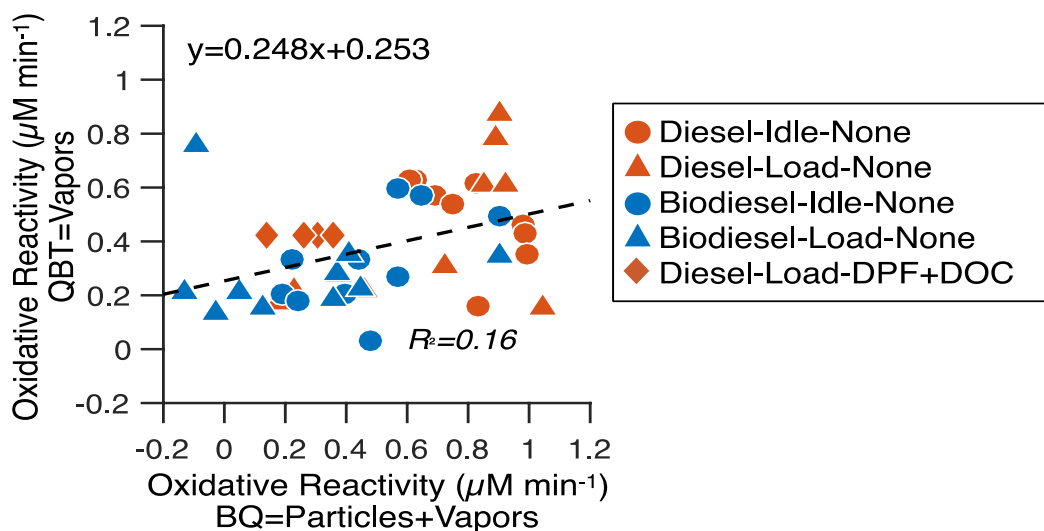


Figure 13: Scatter plot of the raw oxidative reactivity measurements in  $\mu\text{M min}^{-1}$  performed on all paired BQ and QBT filters.

Finally, we did not measure the inorganic and metal species on the filters used to measure the oxidative reactivity and hence were unable to regress the oxidative reactivity against emission factors for the inorganic and metal species. The oxidative reactivity emission factor was highest for Diesel-Idle, followed by Diesel-Load, Biodiesel-Idle, and Biodiesel-None. This can be visualized in Figure 10 where the four different fuel-load combinations are separated on the y-axis with some overlap. Amongst the inorganic and metal species, this order was reproduced by Mg, Cu, Mn, and Pb (see Table 5). Two of these species, namely Cu and Mn that are transition metals, can oxidize DTT efficiently and have been proposed to account for a substantial fraction of oxidative reactivity in ambient samples.<sup>39</sup>

#### **3.5.4 Filter and Solvent Effects**

The filter substrate used to collect particles and the consequent sampling artifacts linked to the filter type are likely to have an influence on the oxidative reactivity measurements. For instance, quartz filters are known to experience both positive and negative artifacts when sampling organic carbon and may bias the mass and composition of the material collected on the filter.<sup>54</sup> The filter medium and the solvent used also likely affect the efficiency with which material collected by the filter is extracted into the solution. For instance, membrane filters have low porosity and collect material on the surface of the filter while fiber filters, which are more porous, collect material inside the fiber matrix. Previous work has found that the oxidative reactivity of PM collected on filters was higher on using a organic solvent (e.g., methanol) for extraction over deionized water.<sup>35,37,60,91</sup> To test the influence of the filter substrate, in this case Teflon<sup>®</sup> versus quartz, we performed additional oxidative reactivity measurements using Teflon<sup>®</sup> filters on a small subset of samples that corresponded to the BQ filters that were already previously analyzed. To test the influence of the solvent, we performed additional oxidative reactivity



measurements on a new set of BQ filters using dichloromethane. The results from those measurements are shown in Figure 14. Although the correlation is quite poor, the oxidative reactivity of DEPs collected on a Teflon<sup>®</sup> filter was approximately twice that collected on a BQ filter (Figure 14(a)). We suspect that because the Teflon<sup>®</sup> filter collects particles on the surface of the filter they might be easier to dislodge during the extraction process and increase the particle concentration in solution. We also saw a strong solvent effect, similar to earlier work, where the use of an organic solvent (i.e., dichloromethane) resulted in a higher oxidative reactivity for both diesel and biodiesel samples (Figure 14(b)). The effect appeared to be much stronger for biodiesel than diesel where the idle and load conditions for diesel were affected differently with the use of the organic solvent.

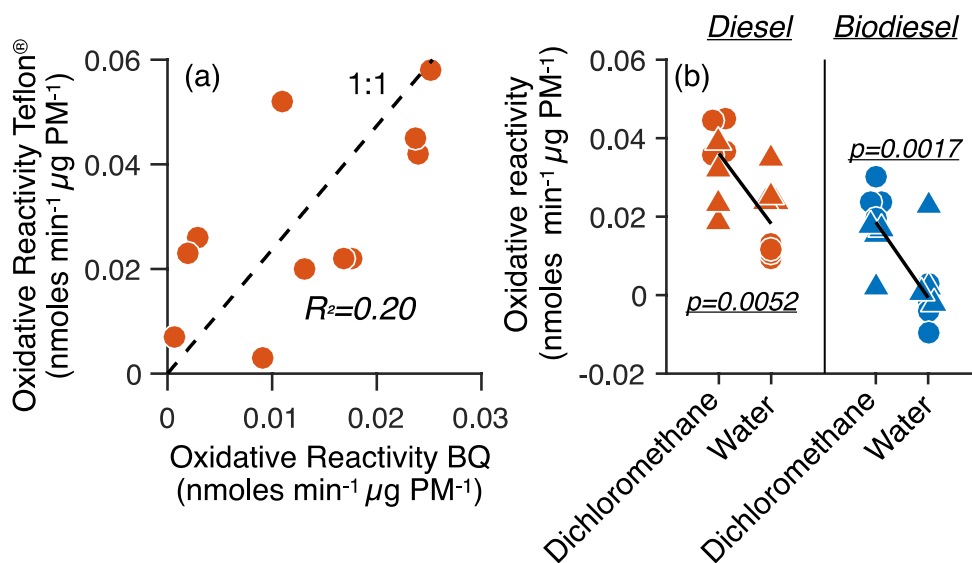


Figure 14: Measured oxidative reactivity of DEPs in  $\text{nmol min}^{-1}\mu\text{g PM}^{-1}$  for select samples examining the influence of the (a) filter type (Teflon<sup>®</sup> versus quartz) and (b) solvent (organic versus water).

#### 4 Discussion and future work

Diesel exhaust particles (DEPs) are an environmental pollutant with well documented impacts on climate and human health. The environmental impacts of DEPs are strongly tied to its composition and properties, which may vary significantly based on the engine type and technology, engine operating conditions, fuel and fuel feedstock, and emissions control technology. In this work, we studied the gas- and particle-phase emissions and composition in diesel exhaust and the semi-volatile fraction and oxidative reactivity of DEPs. These were studied to specifically examine their response to changes in fuel (diesel versus biodiesel), engine load (idle versus 50% load), and emissions control technology (with and without a diesel particle filter (DPF) and diesel oxidation catalyst (DOC)).

The use of soy-based biodiesel, which is the most popular feedstock to produce biodiesel in the United States, resulted in reduced unburned or total hydrocarbons (THC), oxides of nitrogen ( $\text{NO}_x$ ), primary organic aerosol (POA), and elemental carbon (EC) emissions compared to diesel. CO emissions for biodiesel use were lower at idle conditions but higher at load conditions. Largest reductions were observed for EC (62-83%) and the smallest reductions were observed for  $\text{NO}_x$  (6-18%). The use of soy-based biodiesel offers a suitable alternative to diesel fuel by reducing tailpipe emissions of regulated pollutants. As was expected, CO, THC,  $\text{PM}_{2.5}$ , POA, and EC emissions were lower at higher engine loads from higher temperatures in the engine cylinder that reduce incomplete combustion of fuel and lubricating oil.  $\text{NO}_x$  emissions did not seem to be affected much by engine load. The use of an emissions control device (an integrated DPF+DOC) substantially reduced emissions of CO, THC,  $\text{PM}_{2.5}$ , POA, and EC

The use of soy-based biodiesel, different engine loads and emissions control combinations does not seem to alter particle volatility distribution. The amount of DEPs present in atmosphere are abundant and it is important to consider their evolution in atmosphere. This study demonstrates the scope of using one volatility distribution for the same diesel engine regardless of fuel (Diesel or Biodiesel), engine load (idle or 50% load) and emissions control systems (with or without DPF+DOC combination) in atmospheric models.

The oxidative reactivity seems to show overall decreasing oxidative reactivity trends (83 and 93%) for biodiesel fuel and emissions control. The engine load and semi-volatile vapor showed mixed response for units of  $\text{nmol min } \mu\text{g}^{-1} \text{ PM}^{-1}$ . However, the response was stronger when compared on an emission factor basis. The semi-volatile portion contributes approximately 25% of the total oxidative reactivity (particles and vapors combined). The filterable portion of PM does not seem to alter the oxidative reactivity response suggesting reactivity is associated with the component of EC probably quinones (not investigated for this study. In Figure 15, we compare previous oxidative reactivity studies from ambient and source with our findings (references linked to table 6). Our values seemed to be in the range of previous DTT oxidative reactivity studies for both diesel and biodiesel fuel. This study does not use gasoline engine and ambient measurements for DTT assay, but it was worthwhile to see their value ranges from other studies. The value for gasoline PM seems to be in the range of our DTT values. However, the oxidative reactivity of ambient PM was higher when compared with the oxidative reactivity of our measurements. This suggests oxidative reactivity analyzed using DTT assay could possibly be a strong function of composition rather than source type.

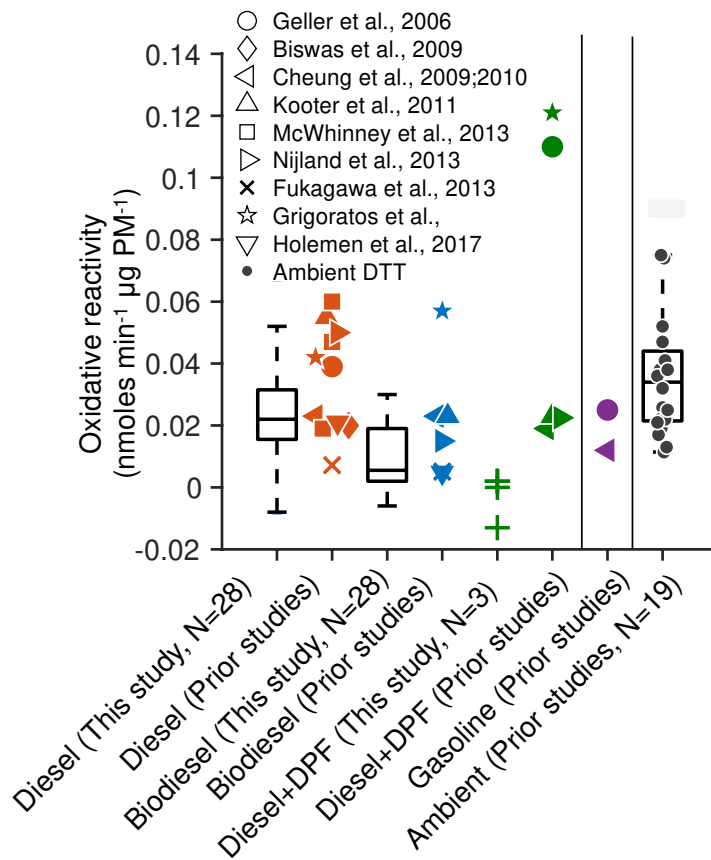


Figure 15: Compares DTT-oxidative reactivity for combustion sources and ambient measurement against our oxidative reactivity data in  $\text{nmoles min}^{-1}\mu\text{g PM}^{-1}$ . The color represents different fuel types and emissions control conditions and different markers are used to represent different source studies. The ambient DTT data shown here is compiled into a box plot from table 5. (For references link to table 5.)

## References

- (1) Pachauri, R. K.; Allen, M. R.; Barros, V. R.; Broome, J.; Cramer, W.; Christ, R.; Church, J. A.; Clarke, L.; Dahe, Q.; Dasgupta, P.; et al. *Climate Change 2014: Synthesis Report. Contribution of Working Groups I, II and III to the Fifth Assessment Report of the Intergovernmental Panel on Climate Change*; Pachauri, R. K., Meyer, L., Eds.; IPCC: Geneva, Switzerland, 2014; p 151.
- (2) Fuzzi, S.; Baltensperger, U.; Carslaw, K.; Decesari, S.; Denier van der Gon, H.; Facchini, M. C.; Fowler, D.; Koren, I.; Langford, B.; Lohmann, U.; et al. Particulate Matter, Air Quality and Climate: Lessons Learned and Future Needs. *Atmos. Chem. Phys.* 2015, 15 (14), 8217–8299.
- (3) Pope, C. A., III; Burnett, R. T.; Krewski, D.; Jerrett, M.; Shi, Y.; Calle, E. E.; Thun, M. J. CLINICAL PERSPECTIVE. *Circulation* 2009, 120 (11), 941–948.
- (4) Anderson, J. O.; Thundiyil, J. G.; Stolbach, A. Clearing the Air: A Review of the Effects of Particulate Matter Air Pollution on Human Health. *J. Med. Toxicol.* 2012, 8 (2), 166–175.
- (5) Albrecht, B. A. Aerosols, Cloud Microphysics, and Fractional Cloudiness. *Science* 1989, 245 (4923), 1227–1230.
- (6) Twomey, S. Pollution and the Planetary Albedo. *Atmos. Environ.* 1974, 8 (12), 1251–1256.
- (7) [PDF]The State of US Health: Innovations, Insights, and Recommendations ..
- (8) Schauer, J. J.; Kleeman, M. J.; Cass, G. R. Measurement of Emissions from Air Pollution Sources. 2. C1 through C30 Organic Compounds from Medium Duty Diesel Trucks. *Sci. Technol. China* 1999.

- (9) Robinson, A. L.; Donahue, N. M.; Shrivastava, M. K.; Weitkamp, E. A.; Sage, A. M.; Grieshop, A. P.; Lane, T. E.; Pierce, J. R.; Pandis, S. N. Rethinking Organic Aerosols: Semivolatile Emissions and Photochemical Aging. *Science* 2007, 315 (5816), 1259–1262.
- (10) May, A. A.; Presto, A. A.; Hennigan, C. J.; Nguyen, N. T.; Gordon, T. D.; Robinson, A. L. Gas-Particle Partitioning of Primary Organic Aerosol Emissions: (1) Gasoline Vehicle Exhaust. *Atmos. Environ.* 2013, 77, 128–139.
- (11) May, A. A.; Presto, A. A.; Hennigan, C. J.; Nguyen, N. T.; Gordon, T. D.; Robinson, A. L. Gas-Particle Partitioning of Primary Organic Aerosol Emissions: (2) Diesel Vehicles. *Environ. Sci. Technol.* 2013, 47 (15), 8288–8296.
- (12) May, A. A.; Levin, E. J. T.; Hennigan, C. J.; Riipinen, I.; Lee, T.; Collett, J. L., Jr.; Jimenez, J. L.; Kreidenweis, S. M.; Robinson, A. L. Gas-Particle Partitioning of Primary Organic Aerosol Emissions: 3. Biomass Burning: BIOMASS-BURNING PARTITIONING. *J. Geophys. Res. D: Atmos.* 2013, 118 (19), 11,327–11,338.
- (13) Pankow, J. F. An Absorption Model of Gas/particle Partitioning of Organic Compounds in the Atmosphere. *Atmos. Environ.* 1994, 28 (2), 185–188.
- (14) Mohr, C.; Huffman, J. A.; Cubison, M. J.; Aiken, A. C.; Docherty, K. S.; Kimmel, J. R.; Ulbrich, I. M.; Hannigan, M.; Jimenez, J. L. Characterization of Primary Organic Aerosol Emissions from Meat Cooking, Trash Burning, and Motor Vehicles with High-Resolution Aerosol Mass Spectrometry and Comparison with Ambient and Chamber Observations. *Environ. Sci. Technol.* 2009, 43 (7), 2443–2449.
- (15) Lipsky, E. M.; Robinson, A. L. Effects of Dilution on Fine Particle Mass and Partitioning of Semivolatile Organics in Diesel Exhaust and Wood Smoke. *Environ. Sci.*

- Technol.* 2006, 40 (1), 155–162.
- (16) Grieshop, A. P.; Logue, J. M.; Donahue, N. M. Laboratory Investigation of Photochemical Oxidation of Organic Aerosol from Wood Fires 1: Measurement and Simulation of Organic Aerosol Evolution. *Atmospheric* 2009.
- (17) Ranjan, M.; Presto, A. A.; May, A. A.; Robinson, A. L. Temperature Dependence of Gas–Particle Partitioning of Primary Organic Aerosol Emissions from a Small Diesel Engine. *Aerosol Sci. Technol.* 2012, 46 (1), 13–21.
- (18) Li, X.; Dallmann, T. R.; May, A. A.; Tkacik, D. S.; Lambe, A. T.; Jayne, J. T.; Croteau, P. L.; Presto, A. A. Gas-Particle Partitioning of Vehicle Emitted Primary Organic Aerosol Measured in a Traffic Tunnel. *Environ. Sci. Technol.* 2016, 50 (22), 12146–12155.
- (19) Weldy, C. S.; Liu, Y.; Liggitt, H. D.; Chin, M. T. In Utero Exposure to Diesel Exhaust Air Pollution Promotes Adverse Intrauterine Conditions, Resulting in Weight Gain, Altered Blood Pressure, and Increased Susceptibility to Heart Failure in Adult Mice. *PLoS One* 2014, 9 (2), e88582.
- (20) Gorr, M. W.; Velten, M.; Nelin, T. D.; Youtz, D. J.; Sun, Q.; Wold, L. E. Early Life Exposure to Air Pollution Induces Adult Cardiac Dysfunction. *Am. J. Physiol. Heart Circ. Physiol.* 2014, 307 (9), H1353–H1360.
- (21) Attfield, M. D.; Schleiff, P. L.; Lubin, J. H.; Blair, A.; Stewart, P. A.; Vermeulen, R.; Coble, J. B.; Silverman, D. T. The Diesel Exhaust in Miners Study: A Cohort Mortality Study with Emphasis on Lung Cancer. *J. Natl. Cancer Inst.* 2012, 104 (11), 869–883.
- (22) Mills, N. L.; Törnqvist, H.; Gonzalez, M. C.; Vink, E.; Robinson, S. D.;

- Söderberg, S.; Boon, N. A.; Donaldson, K.; Sandström, T.; Blomberg, A.; et al. Ischemic and Thrombotic Effects of Dilute Diesel-Exhaust Inhalation in Men with Coronary Heart Disease. *N. Engl. J. Med.* 2007, *357* (11), 1075–1082.
- (23) Ayres, J. G.; Borm, P.; Cassee, F. R.; Castranova, V.; Donaldson, K.; Ghio, A.; Harrison, R. M.; Hider, R.; Kelly, F.; Kooter, I. M.; et al. Evaluating the Toxicity of Airborne Particulate Matter and Nanoparticles by Measuring Oxidative Stress Potential—A Workshop Report and Consensus Statement. *Inhal. Toxicol.* 2008, *20* (1), 75–99.
- (24) Weichenthal, S. A.; Lavigne, E.; Evans, G. J.; Godri Pollitt, K. J.; Burnett, R. T. Fine Particulate Matter and Emergency Room Visits for Respiratory Illness. Effect Modification by Oxidative Potential. *Am. J. Respir. Crit. Care Med.* 2016, *194* (5), 577–586.
- (25) Weichenthal, S.; Lavigne, E.; Evans, G.; Pollitt, K.; Burnett, R. T. Ambient PM<sub>2.5</sub> and Risk of Emergency Room Visits for Myocardial Infarction: Impact of Regional PM<sub>2.5</sub> Oxidative Potential: A Case-Crossover Study. *Environ. Health* 2016, *15*, 46.
- (26) Strak, M.; Janssen, N. A. H.; Godri, K. J.; Gosens, I.; Mudway, I. S.; Cassee, F. R.; Lebret, E.; Kelly, F. J.; Harrison, R. M.; Brunekreef, B.; et al. Respiratory Health Effects of Airborne Particulate Matter: The Role of Particle Size, Composition, and Oxidative Potential—the RAPTES Project. *Environ. Health Perspect.* 2012, *120* (8), 1183–1189.
- (27) Strak, M.; Boogaard, H.; Meliefste, K.; Oldenwening, M.; Zuurbier, M.; Brunekreef, B.; Hoek, G. Respiratory Health Effects of Ultrafine and Fine Particle Exposure in Cyclists. *Occup. Environ. Med.* 2010, *67* (2), 118–124.
- (28) Zuurbier, M.; Hoek, G.; Oldenwening, M.; Meliefste, K.; van den Hazel, P.; Brunekreef, B. Respiratory Effects of Commuters' Exposure to Air Pollution in Traffic.



*Epidemiology* 2011, 22 (2), 219–227.

- (29) Fang, T.; Verma, V.; Bates, J. T.; Abrams, J.; Klein, M.; Strickland, M. J.; Sarnat, S. E.; Chang, H. H.; Mulholland, J. A.; Tolbert, P. E.; et al. Oxidative Potential of Ambient Water-Soluble PM<sub>2.5</sub> in the Southeastern United States: Contrasts in Sources and Health Associations between Ascorbic Acid (AA) and Dithiothreitol (DTT) Assays. *Atmos. Chem. Phys.* 2016, 16 (6), 3865–3879.
- (30) Riva, D. R.; Magalhães, C. B.; Lopes, A. A.; Lanças, T.; Mauad, T.; Malm, O.; Valença, S. S.; Saldiva, P. H.; Faffe, D. S.; Zin, W. A. Low Dose of Fine Particulate Matter (PM<sub>2.5</sub>) Can Induce Acute Oxidative Stress, Inflammation and Pulmonary Impairment in Healthy Mice. *Inhal. Toxicol.* 2011, 23 (5), 257–267.
- (31) Geller, M. D.; Ntziachristos, L.; Mamakos, A.; Samaras, Z.; Schmitz, D. A.; Froines, J. R.; Sioutas, C. Physicochemical and Redox Characteristics of Particulate Matter (PM) Emitted from Gasoline and Diesel Passenger Cars. *Atmos. Environ.* 2006, 40 (36), 6988–7004.
- (32) Biswas, S.; Verma, V.; Schauer, J. J.; Cassee, F. R.; Cho, A. K.; Sioutas, C. Oxidative Potential of Semi-Volatile and Non Volatile Particulate Matter (PM) from Heavy-Duty Vehicles Retrofitted with Emission Control Technologies. *Environ. Sci. Technol.* 2009, 43 (10), 3905–3912.
- (33) Cheung, K. L.; Ntziachristos, L.; Tzamkiozis, T.; Schauer, J. J.; Samaras, Z.; Moore, K. F.; Sioutas, C. Emissions of Particulate Trace Elements, Metals and Organic Species from Gasoline, Diesel, and Biodiesel Passenger Vehicles and Their Relation to Oxidative Potential. *Aerosol Sci. Technol.* 2010, 44 (7), 500–513.

- (34) Kooter, I. M.; van Vugt, M. A. T. M.; Jedynska, A. D.; Tromp, P. C.; Houtzager, M. M. G.; Verbeek, R. P.; Kadijk, G.; Mulderij, M.; Krul, C. A. M. Toxicological Characterization of Diesel Engine Emissions Using Biodiesel and a Closed Soot Filter. *Atmos. Environ.* 2011, *45* (8), 1574–1580.
- (35) McWhinney, R. D.; Badali, K.; Liggio, J.; Li, S.-M.; Abbatt, J. P. D. Filterable Redox Cycling Activity: A Comparison between Diesel Exhaust Particles and Secondary Organic Aerosol Constituents. *Environ. Sci. Technol.* 2013, *47* (7), 3362–3369.
- (36) Stevanovic, S.; Miljevic, B.; Surawski, N. C.; Fairfull-Smith, K. E.; Bottle, S. E.; Brown, R.; Ristovski, Z. D. Influence of Oxygenated Organic Aerosols (OOAs) on the Oxidative Potential of Diesel and Biodiesel Particulate Matter. *Environ. Sci. Technol.* 2013, *47* (14), 7655–7662.
- (37) Verma, V.; Rico-Martinez, R.; Kotra, N.; King, L.; Liu, J.; Snell, T. W.; Weber, R. J. Contribution of Water-Soluble and Insoluble Components and Their Hydrophobic/Hydrophilic Subfractions to the Reactive Oxygen Species-Generating Potential of Fine Ambient Aerosols. *Environ. Sci. Technol.* 2012, *46* (20), 11384–11392.
- (38) Verma, V.; Fang, T.; Guo, H.; King, L.; Bates, J. T.; Peltier, R. E.; Edgerton, E.; Russell, A. G.; Weber, R. J. Reactive Oxygen Species Associated with Water-Soluble PM<sub>2.5</sub> in the Southeastern United States: Spatiotemporal Trends and Source Apportionment. *Atmos. Chem. Phys.* 2014, *14* (23), 12915–12930.
- (39) Charrier, J. G.; Anastasio, C. On Dithiothreitol (DTT) as a Measure of Oxidative Potential for Ambient Particles: Evidence for the Importance of Soluble Transition Metals. *Atmos. Chem. Phys.* 2012, *12* (5), 11317–11350.

- (40) Charrier, J. G.; Richards-Henderson, N. K.; Bein, K. J.; McFall, A. S.; Wexler, A. S.; Anastasio, C. Oxidant Production from Source-Oriented Particulate Matter - Part 1: Oxidative Potential Using the Dithiothreitol (DTT) Assay. *Atmospheric Chemistry & Physics Discussions* 2014, *14*, 24149–24181.
- (41) Saffari, A.; Daher, N.; Shafer, M. M.; Schauer, J. J.; Sioutas, C. Seasonal and Spatial Variation in Dithiothreitol (DTT) Activity of Quasi-Ultrafine Particles in the Los Angeles Basin and Its Association with Chemical Species. *Journal of Environmental Science and Health, Part A* 2014, *49* (4), 441–451.
- (42) Drenth, A. C.; Olsen, D. B.; Cabot, P. E.; Johnson, J. J. Compression Ignition Engine Performance and Emission Evaluation of Industrial Oilseed Biofuel Feedstocks Camelina, Carinata, and Pennycress across Three Fuel Pathways. *Fuel* 2014, *136*, 143–155.
- (43) Performance and Emission Evaluation of Triglyceride-Gasoline Blends in Agricultural Compression Ignition Engines. *Appl. Eng. Agric.* 2014, 523–534.
- (44) Hawley, B.; L'Orange, C.; Olsen, D. B.; Marchese, A. J.; Volckens, J. Oxidative Stress and Aromatic Hydrocarbon Response of Human Bronchial Epithelial Cells Exposed to Petro- or Biodiesel Exhaust Treated with a Diesel Particulate Filter. *Toxicol. Sci.* 2014, *141* (2), 505–514.
- (45) Jathar, S. H.; Friedman, B.; Galang, A. A.; Link, M. F.; Brophy, P.; Volckens, J.; Eluri, S.; Farmer, D. K. Linking Load, Fuel, and Emission Controls to Photochemical Production of Secondary Organic Aerosol from a Diesel Engine. *Environ. Sci. Technol.* 2017, *51* (3), 1377–1386.
- (46) Friedman, B.; Link, M. F.; Fulgham, S. R.; Brophy, P.; Galang, A.; Brune, W. H.;

- Jathar, S. H.; Farmer, D. K. Primary and Secondary Sources of Gas-Phase Organic Acids from Diesel Exhaust. *Environ. Sci. Technol.* 2017, *51* (18), 10872–10880.
- (47) Link, M. F.; Friedman, B.; Fulgham, R.; Brophy, P.; Galang, A.; Jathar, S. H.; Veres, P.; Roberts, J. M.; Farmer, D. K. Photochemical Processing of Diesel Fuel Emissions as a Large Secondary Source of Isocyanic Acid (HNCO): Photochemical Source of Isocyanic Acid. *Geophys. Res. Lett.* 2016, *43* (8), 4033–4041.
- (48) Jathar, S. H.; Heppding, C.; Link, M. F.; Farmer, D. K.; Akherati, A.; Kleeman, M. J.; Gouw, J. A. de; Veres, P. R.; Roberts, J. M. Investigating Diesel Engines as an Atmospheric Source of Isocyanic Acid in Urban Areas. *Atmos. Chem. Phys.* 2017, *17* (14), 8959–8970.
- (49) Schill, G. P.; Jathar, S. H.; Kodros, J. K.; Levin, E. J. T.; Galang, A. M.; Friedman, B.; Link, M. F.; Farmer, D. K.; Pierce, J. R.; Kreidenweis, S. M.; et al. Ice-Nucleating Particle Emissions from Photochemically Aged Diesel and Biodiesel Exhaust: Diesel Exhaust Ice-Nucleating Particles. *Geophys. Res. Lett.* 2016, *43* (10), 5524–5531.
- (50) Hildemann, L. M.; Cass, G. R.; Markowski, G. R. A Dilution Stack Sampler for Collection of Organic Aerosol Emissions: Design, Characterization and Field Tests. *Aerosol Sci. Technol.* 1989, *10* (1), 193–204.
- (51) Ortega, A. M.; Day, D. A.; Cubison, M. J.; Brune, W. H.; Bon, D.; de Gouw, J. A.; Jimenez, J. L. Secondary Organic Aerosol Formation and Primary Organic Aerosol Oxidation from Biomass-Burning Smoke in a Flow Reactor during FLAME-3. *Atmos. Chem. Phys.* 2013, *13* (22), 11551–11571.
- (52) Hinds, W. C. *Aerosol Technology: Properties, Behavior, and Measurement of*

*Airborne Particles*; John Wiley & Sons, 2012.

- (53) Perrino, C.; Canepari, S.; Catrambone, M. Comparing the Performance of Teflon and Quartz Membrane Filters Collecting Atmospheric PM: Influence of Atmospheric Water. *Aerosol Air Qual. Res.* 2013, *13* (1), 137–147.
- (54) Subramanian, R.; Khlystov, A. Y.; Cabada, J. C.; Robinson, A. L. Positive and Negative Artifacts in Particulate Organic Carbon Measurements with Denuded and Undenuded Sampler Configurations Special Issue of Aerosol Science and Technology on Findings from the Fine Particulate Matter Supersites Program. *Aerosol Sci. Technol.* 2004, *38* (sup1), 27–48.
- (55) Lack, D. A.; Lovejoy, E. R.; Baynard, T.; Pettersson, A.; Ravishankara, A. R. Aerosol Absorption Measurement Using Photoacoustic Spectroscopy: Sensitivity, Calibration, and Uncertainty Developments. *Aerosol Sci. Technol.* 2006, *40* (9), 697–708.
- (56) Eller, P. M.; Cassinelli, M. E. Niosh, Elemental Carbon (Diesel Particulate): Method 5040. NIOSH Manual of Analytical Methods. *National Institute for Occupational Safety and Health: Cincinnati, OH, USA* 1996, 2003–2154.
- (57) Birch, M. E.; Cary, R. A. Elemental Carbon-Based Method for Monitoring Occupational Exposures to Particulate Diesel Exhaust. *Aerosol Sci. Technol.* 1996, *25* (3), 221–241.
- (58) [PDF]What Is ICP-MS - USGS.
- (59) De Vizcaya-Ruiz, A.; Gutiérrez-Castillo, M. E.; Uribe-Ramirez, M.; Cebrián, M. E.; Mugica-Alvarez, V.; Sepúlveda, J.; Rosas, I.; Salinas, E.; Garcia-Cuéllar, C.; Martínez,

- F.; et al. Characterization and in Vitro Biological Effects of Concentrated Particulate Matter from Mexico City. *Atmos. Environ.* 2006, 40, 583–592.
- (60) Cho, A. K.; Sioutas, C.; Miguel, A. H.; Kumagai, Y.; Schmitz, D. A.; Singh, M.; Eiguren-Fernandez, A.; Froines, J. R. Redox Activity of Airborne Particulate Matter at Different Sites in the Los Angeles Basin. *Environ. Res.* 2005, 99 (1), 40–47.
- (61) Bein, K. J.; Wexler, A. S. A High-Efficiency, Low-Bias Method for Extracting Particulate Matter from Filter and Impactor Substrates. *Atmos. Environ.* 2014, 90, 87–95.
- (62) Chen, Y.; Bond, T. C. Light Absorption by Organic Carbon from Wood Combustion. *Atmos. Chem. Phys.* 2010, 10 (4), 1773–1787.
- (63) Gundel, L. A.; Dod, R. L.; Rosen, H.; Novakov, T. The Relationship between Optical Attenuation and Black Carbon Concentration for Ambient and Source Particles. *Sci. Total Environ.* 1984, 36, 197–202.
- (64) Hansen, A. D. A.; Rosen, H.; Novakov, T. The Aethalometer — An Instrument for the Real-Time Measurement of Optical Absorption by Aerosol Particles. *Sci. Total Environ.* 1984, 36, 191–196.
- (65) Gordon, T. D.; Presto, A. A.; Nguyen, N. T.; Robertson, W. H.; Na, K.; Sahay, K. N.; Zhang, M.; Maddox, C.; Rieger, P.; Chattopadhyay, S.; et al. Secondary Organic Aerosol Production from Diesel Vehicle Exhaust: Impact of Aftertreatment, Fuel Chemistry and Driving Cycle. *Atmospheric Chemistry & Physics* 2014, 14, 4643–4659.
- (66) Shrivastava, M. K.; Lipsky, E. M.; Stanier, C. O.; Robinson, A. L. Modeling Semivolatile Organic Aerosol Mass Emissions from Combustion Systems. *Environ. Sci.*

*Technol.* 2006, 40 (8), 2671–2677.

- (67) Donahue, N. M.; Robinson, A. L.; Stanier, C. O.; Pandis, S. N. Coupled Partitioning, Dilution, and Chemical Aging of Semivolatile Organics. *Environ. Sci. Technol.* 2006, 40 (8), 2635–2643.
- (68) Turpin, B. J.; Lim, H.-J. Species Contributions to PM<sub>2.5</sub> Mass Concentrations: Revisiting Common Assumptions for Estimating Organic Mass. *Aerosol Sci. Technol.* 2001, 35 (1), 602–610.
- (69) Lapuerta, M.; Rodríguez-Fernández, J.; Agudelo, J. R. Diesel Particulate Emissions from Used Cooking Oil Biodiesel. *Bioresour. Technol.* 2008, 99 (4), 731–740.
- (70) May, A. A.; Nguyen, N. T.; Presto, A. A.; Gordon, T. D.; Lipsky, E. M.; Karve, M.; Gutierrez, A.; Robertson, W. H.; Zhang, M.; Brandow, C.; et al. Gas- and Particle-Phase Primary Emissions from in-Use, on-Road Gasoline and Diesel Vehicles. *Atmos. Environ.* 2014, 88, 247–260.
- (71) Hesterberg, T. W.; Lapin, C. A.; Bunn, W. B. A Comparison of Emissions from Vehicles Fueled with Diesel or Compressed Natural Gas. *Environ. Sci. Technol.* 2008, 42 (17), 6437–6445.
- (72) Robert, M. A.; VanBergen, S.; Kleeman, M. J.; Jakober, C. A. Size and Composition Distributions of Particulate Matter Emissions: Part 1—Light-Duty Gasoline Vehicles. *J. Air Waste Manage. Assoc.* 2007, 57 (12), 1414–1428.
- (73) Herner, J. D.; Hu, S.; Robertson, W. H.; Huai, T.; Chang, M.-C. O.; Rieger, P.; Ayala, A. Effect of Advanced Aftertreatment for PM and NO<sub>x</sub> Reduction on Heavy-Duty

- Diesel Engine Ultrafine Particle Emissions. *Environ. Sci. Technol.* 2011, 45 (6), 2413–2419.
- (74) Volckens, J.; Olson, D. A.; Hays, M. D. Carbonaceous Species Emitted from Handheld Two-Stroke Engines. *Atmos. Environ.* 2008, 42 (6), 1239–1248.
- (75) Dallmann, T. R.; Harley, R. A.; Kirchstetter, T. W. Effects of Diesel Particle Filter Retrofits and Accelerated Fleet Turnover on Drayage Truck Emissions at the Port of Oakland. *Environ. Sci. Technol.* 2011, 45 (24), 10773–10779.
- (76) Shah, S. D.; Cocker, D. R.; Miller, J. W.; Norbeck, J. M. Emission Rates of Particulate Matter and Elemental and Organic Carbon from In-Use Diesel Engines. *Environ. Sci. Technol.* 2004, 38 (9), 2544–2550.
- (77) Fujita, E. M.; Campbell, D. E.; Zielinska, B.; Chow, J. C.; Lindhjem, C. E.; DenBleyker, A.; Bishop, G. A.; Schuchmann, B. G.; Stedman, D. H.; Lawson, D. R. Comparison of the MOVES2010a, MOBILE6.2, and EMFAC2007 Mobile Source Emission Models with on-Road Traffic Tunnel and Remote Sensing Measurements. *J. Air Waste Manag. Assoc.* 2012, 62 (10), 1134–1149.
- (78) Dallmann, T. R.; DeMartini, S. J.; Kirchstetter, T. W.; Herndon, S. C.; Onasch, T. B.; Wood, E. C.; Harley, R. A. On-Road Measurement of Gas and Particle Phase Pollutant Emission Factors for Individual Heavy-Duty Diesel Trucks. *Environ. Sci. Technol.* 2012, 46 (15), 8511–8518.
- (79) Grieshop, A. P.; Lipsky, E. M.; Pekney, N. J.; Takahama, S.; Robinson, A. L. Fine Particle Emission Factors from Vehicles in a Highway Tunnel: Effects of Fleet Composition and Season. *Atmos. Environ.* 2006, 40, 287–298.



- (80) Demirbas, A. Biofuels Sources, Biofuel Policy, Biofuel Economy and Global Biofuel Projections. *Energy Convers. Manage.* 2008, 49 (8), 2106–2116.
- (81) Aiken, A. C.; DeCarlo, P. F.; Kroll, J. H.; Worsnop, D. R.; Huffman, J. A.; Docherty, K. S.; Ulbrich, I. M.; Mohr, C.; Kimmel, J. R.; Sueper, D.; et al. O/C and OM/OC Ratios of Primary, Secondary, and Ambient Organic Aerosols with High-Resolution Time-of-Flight Aerosol Mass Spectrometry. *Environ. Sci. Technol.* 2008, 42 (12), 4478–4485.
- (82) Chow, J. C.; Watson, J. G.; Chen, L. W. A.; Arnott, W. P.; Moosmüller, H.; Fung, K. Equivalence of Elemental Carbon by Thermal/optical Reflectance and Transmittance with Different Temperature Protocols. *Environ. Sci. Technol.* 2004, 38 (16), 4414–4422.
- (83) Cavalli, F.; Viana, M.; Yttri, K. E.; Genberg, J.; Putaud, J.-P. Toward a Standardised Thermal-Optical Protocol for Measuring Atmospheric Organic and Elemental Carbon: The EUSAAR Protocol. *Atmospheric Measurement Techniques* 2010, 3 (1), 79–89.
- (84) Epstein, S. A.; Riipinen, I.; Donahue, N. M. A Semiempirical Correlation between Enthalpy of Vaporization and Saturation Concentration for Organic Aerosol. *Environ. Sci. Technol.* 2010, 44 (2), 743–748.
- (85) Gerlofs-Nijland, M. E.; Totlandsdal, A. I.; Tzamkiozis, T.; Leseman, D. L. A. C.; Samaras, Z.; Låg, M.; Schwarze, P.; Ntziachristos, L.; Cassee, F. R. Cell Toxicity and Oxidative Potential of Engine Exhaust Particles: Impact of Using Particulate Filter or Biodiesel Fuel Blend. *Environ. Sci. Technol.* 2013, 47 (11), 5931–5938.
- (86) Holmen, B. A.; Rukavina, B.; Kasumba, J. Reactive Oxidative Species and Speciated Particulate Light-Duty Engine Emissions from Diesel and Biodiesel Fuel Blends. *Energy* 2017.

- (87) Fukagawa, N. K.; Li, M.; Poynter, M. E.; Palmer, B. C.; Parker, E.; Kasumba, J.; Holmén, B. A. Soy Biodiesel and Petrodiesel Emissions Differ in Size, Chemical Composition and Stimulation of Inflammatory Responses in Cells and Animals. *Environ. Sci. Technol.* 2013, *47* (21), 12496–12504.
- (88) Grigoratos, T.; Fontaras, G.; Kalogirou, M.; Samara, C.; Samaras, Z.; Rose, K. Effect of Rapeseed Methyl ester Blending on Diesel Passenger Car Emissions – Part 2: Unregulated Emissions and Oxidation Activity. *Fuel* 2014, *Complete* (128), 260–267.
- (89) Betha, R.; Pavagadhi, S.; Sethu, S.; Hande, M. P.; Balasubramanian, R. Comparative in Vitro Cytotoxicity Assessment of Airborne Particulate Matter Emitted from Stationary Engine Fuelled with Diesel and Waste Cooking Oil-Derived Biodiesel. *Atmos. Environ.* 2012, *61*, 23–29.
- (90) Pourkhesalian, A. M.; Stevanovic, S.; Salimi, F.; Rahman, M. M.; Wang, H.; Pham, P. X.; Bottle, S. E.; Masri, A. R.; Brown, R. J.; Ristovski, Z. D. Influence of Fuel Molecular Structure on the Volatility and Oxidative Potential of Biodiesel Particulate Matter. *Environ. Sci. Technol.* 2014, *48* (21), 12577–12585.
- (91) Gao, D.; Fang, T.; Verma, V.; Zeng, L.; Weber, R. J. A Method for Measuring Total Aerosol Oxidative Potential (OP) with the Dithiothreitol (DTT) Assay and Comparisons between an Urban and Roadside Site of Water-Soluble and Total OP. *Atmospheric Measurement Techniques* 2017, *10* (8), 2821–2835.

## Appendix

Table 6: Compilation of DTT-based oxidative reactivity measurements from engine and vehicle tests and ambient sampling.

<i>Engine or Vehicle Testing</i>			
<i>Study</i>	<i>Source</i>	<i>Feedstock</i>	<i>DTT oxidative reactivity</i>
Geller et al., 2006	Euro 3 diesel vehicle	Conventional diesel (8 ppm sulfur)	0.034-0.043 nmoles min <sup>-1</sup> μg <sup>-1</sup>
	Euro 3 gasoline vehicle	Conventional gasoline (<50 ppm sulfur)	0.022-0.028 nmoles min <sup>-1</sup> μg <sup>-1</sup>
	Euro 4 diesel vehicle	Conventional diesel (8 ppm sulfur)	0.108-0.112 nmoles min <sup>-1</sup> μg <sup>-1</sup>
Biswas et al., 2009	Heavy-duty vehicle (no emissions control)	Ultra low sulfur diesel fuel (<15 ppm sulfur)	0.018-0.021 nmoles min <sup>-1</sup> μg <sup>-1</sup>
	Heavy-duty vehicle (w/ emissions control)	Ultra low sulfur diesel fuel (<15 ppm sulfur)	0.01-0.185 nmoles min <sup>-1</sup> μg <sup>-1</sup>
Cheung et al., 2009; 2010	Euro 2 diesel vehicle	Diesel (<50 ppm sulfur)	0.009-0.029 nmoles min <sup>-1</sup> μg <sup>-1</sup>
	Euro 2 soy biodiesel vehicle	Soy Biodiesel (sulfur free)	0.0016-0.034 nmoles min <sup>-1</sup> μg <sup>-1</sup>
	Euro 3 gasoline vehicle	Gasoline (50 ppm sulfur)	0.009-0.015 nmoles min <sup>-1</sup> μg <sup>-1</sup>
	Euro 4 diesel vehicle	Diesel (<10 ppm sulfur)	0.013-0.025 nmoles min <sup>-1</sup> μg <sup>-1</sup>
Kooter et al., 2011	Heavy-duty vehicle (B0 to B20, no DPF)	Conventional diesel (10 ppm sulfur)	0.046-0.064 nmoles min <sup>-1</sup> μg <sup>-1</sup>
	Heavy-duty vehicle (B100, DPF)	~likely soy Biodiesel (10 ppm sulfur)	0.022-0.025 nmoles min <sup>-1</sup> μg <sup>-1</sup>
McWhinney et al., 2013	Tier 1 light-duty diesel vehicle	Ultra low sulfur diesel fuel	0.02-0.06 nmoles min <sup>-1</sup> μg <sup>-1</sup>
Nijland et al.,	Euro 4 diesel vehicle w/o DPF (B0)	Neat diesel (10 ppm)	0.04-0.09 nmoles

2013		sulfur)	$\text{min}^{-1} \mu\text{g}^{-1}$
	Euro 4 diesel vehicle w/o DPF (B50)	Rapeseed Biodiesel (10 ppm sulfur)	0.006-0.02 nmoles $\text{min}^{-1} \mu\text{g}^{-1}$
	Euro 4 diesel vehicle w/ DPF (B0)	Neat diesel (10 ppm sulfur)	0.003 nmoles $\text{min}^{-1} \mu\text{g}^{-1}$
	Euro 4 diesel vehicle w/ DPF (B50)	Rapeseed Biodiesel (10 ppm sulfur)	0.005-0.02 nmoles $\text{min}^{-1} \mu\text{g}^{-1}$
Fukagawa et al., 2013	Light-duty diesel engine (B0)	Ultra low sulfur petrodiesel (1.2 ppm sulfur)	0.0072 nmoles $\text{min}^{-1} \mu\text{g}^{-1}$
	Light-duty diesel engine blend (B20)	Soy Biodiesel	0.0051 nmoles $\text{min}^{-1} \mu\text{g}^{-1}$
Grigoratos et al., 2014	Euro 4 Diesel engine w/ DOC on NEDC cycle (B0)	Base diesel fuel (10 ppm sulfur)	0.012-0.072 nmoles $\text{min}^{-1} \mu\text{g}^{-1}$
	Euro 4 Diesel engine w/ DPF+DOC on NEDC cycle (B0)	Base diesel fuel (10 ppm sulfur)	0.046-0.196 nmoles $\text{min}^{-1} \mu\text{g}^{-1}$
	Euro 4 Diesel engine w/ DOC NEDC cycle (B50)	Rapeseed Biodiesel (10 ppm sulfur)	0.009-0.105 nmoles $\text{min}^{-1} \mu\text{g}^{-1}$
	Euro 4 Diesel engine w/ DPF+DOC on NEDC cycle (B50)	Rapeseed Biodiesel (10 ppm sulfur)	0.111-0.165 nmoles $\text{min}^{-1} \mu\text{g}^{-1}$
Holmen et al., 2017	Light duty engine	Diesel (10 ppm sulfur)	0.0083-0.035 nmoles $\text{min}^{-1} \mu\text{g}^{-1}$
	Light duty engine (B100)	Soy biodiesel	0.0022-0.025 nmoles $\text{min}^{-1} \mu\text{g}^{-1}$
	Light duty engine	Diesel (10 ppm sulfur)	0.0091-0.0361 nmoles $\text{min}^{-1} \mu\text{g}^{-1}$
	Light duty engine (B100)	Waste vegetable oil biodiesel	0.0001-0.0169 nmoles $\text{min}^{-1} \mu\text{g}^{-1}$
<i>Ambient Sampling</i>			
<i>Study</i>	<i>Source</i>		<i>DTT oxidative reactivity</i>
Ruiz et al., 2006	Mexico city, 2003 (PM <sub>2.5</sub> )		0.015-0.04 nmoles $\text{min}^{-1} \mu\text{g}^{-1}$

	Mexico city, 2003 (PM <sub>2.5-10</sub> )	0.005-0.015 nmoles min <sup>-1</sup> μg <sup>-1</sup>
Ntziachristos et al., 2007	South Coast Air Basin, 2003-2005 (PM <sub>0.15</sub> )	0.042-0.172 nmoles min <sup>-1</sup> μg <sup>-1</sup>
	South Coast Air Basin, 2003-2005 (PM <sub>0.15-2.5</sub> )	0.021-0.075 nmoles min <sup>-1</sup> μg <sup>-1</sup>
Hu et al., 2008	Los Angeles-Long Beach, 2007 (PM <sub>0.25</sub> )	0.031-0.055 nmoles min <sup>-1</sup> μg <sup>-1</sup>
	Los Angeles-Long Beach, 2007 (PM <sub>0.25-2.5</sub> )	0.018-0.024 nmoles min <sup>-1</sup> μg <sup>-1</sup>
	Los Angeles-Long Beach, 2007 (PM <sub>2.5-10</sub> )	0.008-0.018 nmoles min <sup>-1</sup> μg <sup>-1</sup>
Verma et al., 2009a	Los Angeles during wildfires, 2007	0.014-0.024 nmoles min <sup>-1</sup> μg <sup>-1</sup>
Verma et al., 2009b	Los Angeles, 2008 (Morning)	0.022-0.07 nmoles min <sup>-1</sup> μg <sup>-1</sup>
	Los Angeles, 2008 (Afternoon)	0.062-0.12 nmoles min <sup>-1</sup> μg <sup>-1</sup>
Charrier et al., 2012	San Joaquin Valley - Fresno, 2006 (urban)	0.027-0.061 nmoles min <sup>-1</sup> μg <sup>-1</sup>
	San Joaquin Valley - Westside, 2009 (rural)	0.020-0.025 nmoles min <sup>-1</sup> μg <sup>-1</sup>
Verma et al., 2012	Atlanta, 2012 (water extract)	0.012-0.032 nmoles min <sup>-1</sup> μg <sup>-1</sup>
	Atlanta, 2012 (methanol extract)	0.02-0.055 nmoles min <sup>-1</sup> μg <sup>-1</sup>
Verma et al., 2014	Southeast US, 2012-2013	0.01-0.05 nmoles min <sup>-1</sup> μg <sup>-1</sup>
Charrier et al., 2015	Vehicle emissions summer (ultrafine)	0.015-0.025 nmoles min <sup>-1</sup> μg <sup>-1</sup>
	Vehicle emissions winter (ultrafine)	0.02-0.05 nmoles min <sup>-1</sup> μg <sup>-1</sup>
Vreeland et al., 2017	Atlanta, 2012-2013 (inside vehicle)	0.006-0.39 nmoles min <sup>-1</sup> μg <sup>-1</sup>
	Atlanta, 2012-2013 (roadside)	0.004-0.014

		nmoles min <sup>-1</sup> μg <sup>-1</sup>
--	--	---

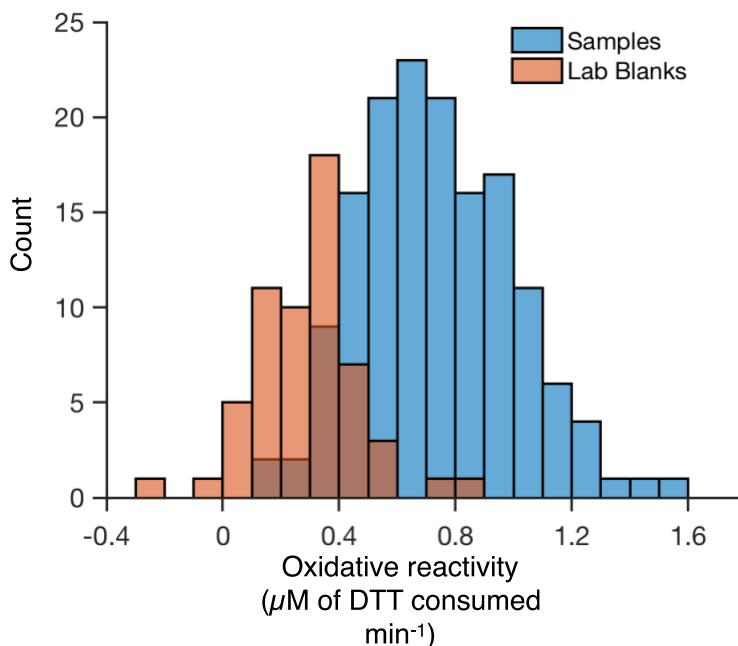


Figure 16: Compares histogram plot for all sample and laboratory measurements in units of  $\mu\text{M}$  of DTT consumed  $\text{min}^{-1}$ .

In Figure 16, we compare histogram plot for both laboratory blanks and actual oxidative reactivity measurements of DEP's. The laboratory blanks here are the raw consumption DTT activity associated to the sample solution without any  $\text{PM}_{2.5}$ . The oxidative reactivity of our lab blanks was found to be more for a total of 12 samples. This was potentially one of the reason of negative oxidative reactivity data in our plots. DTT assay analysis done on handling and dynamic blanks, also adds up to this higher lab blanks, creating negative data in our study. We would treat negative data equivalent to zero for this study.